



CERN-EP-2017-254
 LHCb-PAPER-2017-037
 07 December 2017

Measurement of the B^\pm production cross-section in pp collisions at $\sqrt{s} = 7$ and 13 TeV

LHCb collaboration[†]

Abstract

The production of B^\pm mesons is studied in pp collisions at centre-of-mass energies of 7 and 13 TeV, using $B^\pm \rightarrow J/\psi K^\pm$ decays and data samples corresponding to 1.0 fb^{-1} and 0.3 fb^{-1} , respectively. The production cross-sections summed over both charges and integrated over the transverse momentum range $0 < p_T < 40\text{ GeV}/c$ and the rapidity range $2.0 < y < 4.5$ are measured to be

$$\begin{aligned}\sigma(pp \rightarrow B^\pm X, \sqrt{s} = 7\text{ TeV}) &= 43.0 \pm 0.2 \pm 2.5 \pm 1.7\text{ }\mu\text{b}, \\ \sigma(pp \rightarrow B^\pm X, \sqrt{s} = 13\text{ TeV}) &= 86.6 \pm 0.5 \pm 5.4 \pm 3.4\text{ }\mu\text{b},\end{aligned}$$

where the first uncertainties are statistical, the second are systematic, and the third are due to the limited knowledge of the $B^\pm \rightarrow J/\psi K^\pm$ branching fraction. The ratio of the cross-section at 13 TeV to that at 7 TeV is determined to be $2.02 \pm 0.02\text{ (stat)} \pm 0.12\text{ (syst)}$. Differential cross-sections are also reported as functions of p_T and y . All results are in agreement with theoretical calculations based on the state-of-art fixed next-to-leading order quantum chromodynamics.

Published in JHEP 12 (2017) 026

© CERN on behalf of the LHCb collaboration, licence CC-BY-4.0.

[†]Authors are listed at the end of this paper.

1 Introduction

Precise measurements of the production cross-section of B^\pm mesons in pp collisions provide important tests of perturbative quantum chromodynamics (QCD) calculations, particularly of the state-of-the-art calculations based on the fixed next-to-leading order (NLO) QCD with next-to-leading logarithm (NLL) large transverse momentum resummation (FONLL) approach [1, 2]. The FONLL calculations are accurate to the full NLO level at moderate p_T values, and to the NLL level at high p_T . The FONLL predictions are then achieved by properly merging a ‘massless’ resummed approach, valid in the high p_T region, with a full massive fixed-order calculation, reliable in the small p_T region. The ratio of cross-sections between different centre-of-mass energies is of particular interest due to cancellations that occur in the theoretical and experimental uncertainties. Uncertainties arising from assumptions about the values of the FONLL parameters largely cancel in the ratio. Experimentally, uncertainties due to factors such as the branching fractions of decays and the b -quark fragmentation fractions [3] to specific hadrons are highly correlated at different beam energies and their effect is much reduced in the ratio.

Previous measurements of B^\pm production have been performed in different kinematic regions at the centre-of-mass energy $\sqrt{s} = 7\text{ TeV}$ by several experiments at the Large Hadron Collider. The CMS collaboration reported the integrated and differential B^\pm production cross-sections in the range $p_T > 5\text{ GeV}/c$ and $|y| < 2.4$ [4, 5], where p_T and y are the component of the momentum transverse to the beam line and the rapidity of the B^\pm mesons, respectively. The ATLAS collaboration measured the production cross-sections in the range $9 < p_T < 120\text{ GeV}/c$ and $|y| < 2.25$ [6]. The LHCb collaboration measured the integrated and differential cross-sections for B^\pm with $0 < p_T < 40\text{ GeV}/c$ and $2.0 < y < 4.5$ using a data sample collected in 2010 that corresponds to an integrated luminosity of 35 pb^{-1} [7]. This result was later updated using a data sample collected in early 2011, corresponding to an integrated luminosity of 362 pb^{-1} [8].

This article updates the previous LHCb results using a larger data sample collected in 2011 with the LHCb experiment at $\sqrt{s} = 7\text{ TeV}$ and corresponding to an integrated luminosity of 1.0 fb^{-1} . The first measurements of the integrated and differential cross-sections of B^\pm mesons at $\sqrt{s} = 13\text{ TeV}$ are also presented, using a data sample collected in 2015 and corresponding to an integrated luminosity of 0.3 fb^{-1} . Following the previous LHCb measurements [7, 8], the B^\pm mesons are reconstructed in the $B^\pm \rightarrow J/\psi K^\pm$ mode followed by $J/\psi \rightarrow \mu^+\mu^-$ and the production cross-sections are measured in the range $0 < p_T < 40\text{ GeV}/c$ and $2.0 < y < 4.5$. The ratio of the cross-sections in the 13 TeV and 7 TeV data is also measured as a function of p_T and y .

2 Event selection

The LHCb detector [9, 10] is a single-arm forward spectrometer covering the pseudorapidity range $2 < \eta < 5$, designed for the study of particles containing b or c quarks. The detector includes a high-precision tracking system consisting of a silicon-strip vertex detector surrounding the pp interaction region, a large-area silicon-strip detector located upstream of a dipole magnet with a bending power of about 4 Tm , and three stations of silicon-strip detectors and straw drift tubes placed downstream of the magnet. The tracking system provides a measurement of momentum, p , of charged particles with a relative uncertainty

that varies from 0.5% at low momentum to 1.0% at $200\text{ GeV}/c$. The minimum distance of a track to a primary vertex, the impact parameter, is measured with a resolution of $(15 + 29/p_T)\mu\text{m}$, where p_T is in units of GeV/c . Different types of charged hadrons are distinguished using information from two ring-imaging Cherenkov detectors. Photons, electrons and hadrons are identified by a calorimeter system consisting of scintillating-pad (SPD) and preshower detectors, an electromagnetic calorimeter and a hadronic calorimeter. Muons are identified by a system composed of alternating layers of iron and multiwire proportional chambers.

The online event selection is performed by a trigger, which consists of a hardware stage (L0), based on information from the calorimeter and muon systems, followed by a two-stage software-based high-level trigger (HLT1, HLT2) [11], where the HLT1 stage uses partial event reconstruction to reduce the rate and the HLT2 stage applies a full event reconstruction. At the hardware stage, events are required to have a dimuon candidate with large p_T , while at the software stage the dimuon invariant mass is required to be consistent with the known J/ψ mass [12]. Finally, a set of global event cuts (GEC) is applied in order to prevent high-multiplicity events from dominating the processing time of the software trigger, which includes the requirement that the number of hits in the SPD subdetector should be less than 900.

Simulated events are used to optimise the selection, determine some of the efficiencies and estimate the background contamination. The simulation is based on the PYTHIA8 generator [13] with a specific LHCb configuration [14]. Decays of hadrons are described by EVTGEN [15], in which final-state radiation is generated using PHOTOS [16]. The interaction of the generated particles with the detector, and its response, are implemented using the GEANT4 toolkit [17], as described in Ref. [18].

The B^\pm candidates are made by combining J/ψ and K^\pm candidates. The offline event selection forms J/ψ candidates using pairs of muons with opposite charge. The muon candidates must have $p_T > 700\text{ MeV}/c$, and satisfy track-reconstruction quality and particle identification (PID) requirements. The muon pair is required to be consistent with originating from a common vertex [19] and have an invariant mass, $M(\mu\mu)$, within the range $3.04 < M(\mu\mu) < 3.14\text{ GeV}/c^2$. The K^\pm candidates are required to have p_T greater than $500\text{ MeV}/c$ and satisfy track-reconstruction quality requirements. No PID requirement is applied to select the kaon, as the only topologically similar decay, $B^\pm \rightarrow J/\psi\pi^\pm$, is Cabibbo suppressed.

The three tracks in the final state of the B^\pm decay are required to form a common vertex with a good vertex-fit quality. In order to suppress background due to the random combination of particles produced in the pp interactions, the B^\pm candidates are required to have a decay time larger than 0.3 ps . Finally, B^\pm candidates with $0 < p_T < 40\text{ GeV}/c$ and $2.0 < y < 4.5$ are selected for subsequent analysis.

3 Cross-section determination

The differential production cross-section of B^\pm mesons is measured as a function of p_T and y using

$$\frac{d^2\sigma}{dydp_T} = \frac{N_{B^\pm}}{\mathcal{L} \times \varepsilon_{\text{tot}} \times \mathcal{B}(B^\pm \rightarrow J/\psi K^\pm) \times \mathcal{B}(J/\psi \rightarrow \mu^+\mu^-) \times \Delta y \times \Delta p_T}, \quad (1)$$

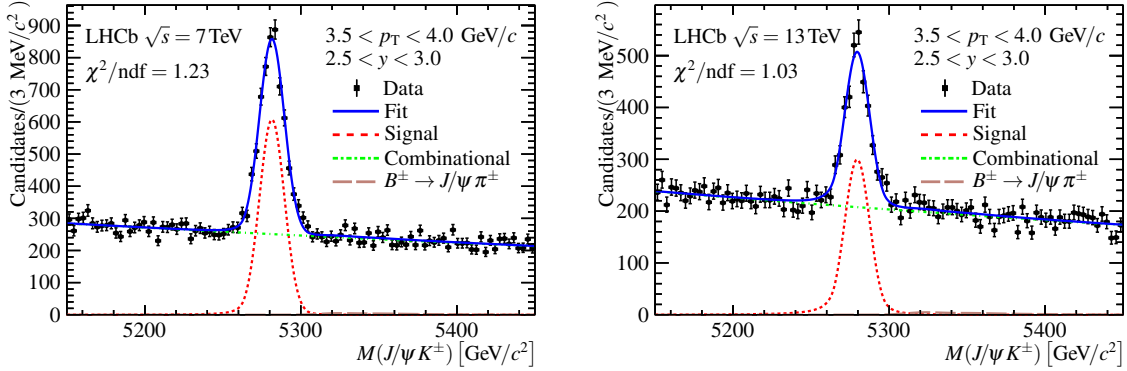


Figure 1: Invariant mass distributions of B^\pm candidates in the range $3.5 < p_T < 4.0 \text{ GeV}/c$ and $2.5 < y < 3.0$ using (left) 7 TeV and (right) 13 TeV data. The black points are the number of selected candidates in each bin, the blue curve represents the fit result, the red-dotted line represents the $B^\pm \rightarrow J/\psi K^\pm$ signal, and the green- and brown-dashed lines are contributions from the combinatorial and the Cabibbo-suppressed backgrounds. The Cabibbo-suppressed background contribution $B^\pm \rightarrow J/\psi \pi^\pm$ is only just visible at masses above the signal peak.

where N_{B^\pm} is the number of reconstructed $B^\pm \rightarrow J/\psi K^\pm$ candidates in a given (p_T , y) bin after background subtraction, \mathcal{L} is the integrated luminosity, ε_{tot} is the bin-dependent total efficiency, $\mathcal{B}(B^\pm \rightarrow J/\psi K^\pm)$ is the branching fraction of B^\pm decays to $J/\psi K^\pm$ [20, 21], $\mathcal{B}(J/\psi \rightarrow \mu^+ \mu^-)$ is the branching fraction of J/ψ decays to $\mu^+ \mu^-$ [12], and Δy and Δp_T are the bin widths in y and p_T . The value of $\mathcal{B}(B^\pm \rightarrow J/\psi K^\pm)$ is calculated to be $(1.044 \pm 0.040) \times 10^{-3}$ by combining the two exclusive measurements from the Belle [20] and BaBar [21] collaborations, under the assumption that only the uncertainty for $J/\psi \rightarrow \mu^+ \mu^-$ branching fraction is correlated.

The yield of $B^\pm \rightarrow J/\psi K^\pm$ decays in each (p_T , y) bin is obtained independently by fitting the invariant mass distribution of the B^\pm candidates, $M(J/\psi K^\pm)$, in the interval $5150 < M(J/\psi K^\pm) < 5450 \text{ MeV}/c^2$, using an extended unbinned maximum likelihood fit. The $M(J/\psi K^\pm)$ distribution is described by a probability density function (PDF) consisting of the following three components: a modified Crystal Ball (CB) function [22] to model the signal, an exponential function to model the combinatorial background, and a double CB function to model the contamination from the Cabibbo suppressed decay $B^\pm \rightarrow J/\psi \pi^\pm$, where the charged pion is misidentified as a kaon. The modified CB function used for the signal component has tails on both the low- and the high-mass side of the peak, which are described by separate parameters. In each bin, the tail parameters are determined from simulation, leaving the mean and width as free parameters. The shape of the misidentification background is obtained using simulated $B^\pm \rightarrow J/\psi \pi^\pm$ decays that satisfy the selection criteria for the decay $B^\pm \rightarrow J/\psi K^\pm$, and the yield of the misidentification background is determined according to the branching fraction ratio $\mathcal{B}(B^\pm \rightarrow J/\psi \pi^\pm)/\mathcal{B}(B^\pm \rightarrow J/\psi K^\pm)$ from Ref. [12]. Figure 1 shows, as an example, the invariant mass distribution of the B^\pm candidates in the range $3.5 < p_T < 4.0 \text{ GeV}/c$ and $2.5 < y < 3.0$.

The total efficiency, ε_{tot} , is the product of several efficiencies and can be written as

$$\varepsilon_{\text{tot}} = \varepsilon_{\text{acc}} \times \varepsilon_{\text{reco\&sel}} \times \varepsilon_{\text{PID}} \times \varepsilon_{\text{track}} \times \varepsilon_{\text{trigger}} \times \varepsilon_{\text{GEC}}. \quad (2)$$

The acceptance factor, ε_{acc} , is the fraction of signal with all final-state particles within the

Table 1: Summary of relative systematic uncertainties on the integrated production cross-sections at $\sqrt{s} = 7$ and 13 TeV, and the ratio of the cross-sections $R(13 \text{ TeV}/7 \text{ TeV})$.

Sources	Uncertainty (%)		
	7 TeV	13 TeV	$R(13 \text{ TeV}/7 \text{ TeV})$
Luminosity	1.7	3.9	3.4
Branching fractions	3.9	3.9	0.0
Binning	2.6	2.7	0.0
Mass fits	2.7	1.3	1.5
Acceptance	0.2	0.1	0.2
Reconstruction	0.1	0.1	0.2
Track	1.6	2.6	1.0
PID	0.4	0.1	0.4
Trigger	3.5	2.6	4.4
GEC	0.7	0.7	1.0
Selection	1.0	1.1	0.1
Weighting	0.2	0.2	0.3
Total	7.0	7.4	5.9

fiducial region of the detector acceptance, and is calculated from simulation, as shown in Appendix A. The efficiency of the particle reconstruction and event selection, $\varepsilon_{\text{reco}\&\text{sel}}$, is also determined from simulation. The efficiency of identifying the two muons in the final state, ε_{PID} , and the track finding efficiency, $\varepsilon_{\text{track}}$, are measured using a tag-and-probe method [23, 24] on a control data sample of $J/\psi \rightarrow \mu^+ \mu^-$ decays. The trigger efficiency, $\varepsilon_{\text{trigger}}$, is estimated in two parts, which are $\varepsilon_{\text{L0}\&\text{HLT1}}$ and $\varepsilon_{\text{HLT2}}$. The $\varepsilon_{\text{L0}\&\text{HLT1}}$ efficiency is evaluated by estimating the fraction of events in a trigger-unbiased data sample that satisfy the trigger requirements, and the $\varepsilon_{\text{HLT2}}$ efficiency is evaluated using simulated signal events, as the effects of HLT2 trigger are well modelled. The GEC efficiency, ε_{GEC} , is measured to be $(99.2 \pm 0.1)\%$ for the 7 TeV and $(99.3 \pm 0.1)\%$ for the 13 TeV data sample, and is independent of p_T and y . It is extracted by fitting the SPD multiplicity distribution and extrapolating the function to determine the fraction of events that are accepted. The measured ε_{tot} are tabulated in Appendix B.

4 Systematic uncertainties

Sources of systematic uncertainty associated with the determination of the luminosity, branching fractions, signal yields, efficiencies, along with their effects on the integrated cross-section measurements, are summarised in Table 1. The total systematic uncertainty is obtained from the sum in quadrature of all contributions. Several uncertainties have been reduced in the $\sqrt{s} = 13$ TeV measurement, due to a larger simulation sample and a better understanding of the efficiency.

Following the procedures used in Ref. [25], the relative uncertainty on the luminosity is determined to be 1.7% for the 7 TeV data and 3.9% for the 13 TeV data sample. The relative uncertainty on $\mathcal{B}(B^\pm \rightarrow J/\psi K^\pm)$ is 3.9% [20, 21], while the uncertainty on $\mathcal{B}(J/\psi \rightarrow \mu^+ \mu^-)$ [12] is negligible.

The variation of the efficiency within a bin induces an uncertainty if the kinematic distributions of the simulated samples do not match those of the data. This uncertainty, which is important close to the edges of the fiducial region, is estimated by increasing or decreasing the bin width in p_T and y by a factor of two. The largest variation of the integrated cross-section measurement is taken as a systematic uncertainty on the production cross-sections.

The systematic uncertainty associated with the invariant mass fits is obtained by performing fits using alternative choices for the signal and background functions. The signal PDF is replaced by a HYPATIA function [26], while the combinatorial background model is modified to be either a first-order or second-order polynomial function. The largest resulting variation of the cross-section measurement is taken as a systematic uncertainty.

The efficiencies of the tracking, PID and trigger are estimated using control samples, and systematic uncertainties arise due to the limited sample sizes. An additional uncertainty arises on the track-reconstruction efficiency due to limited knowledge of the material budget of the detector, which induces a 1.1% uncertainty on the kaon reconstruction efficiency due to modelling of hadronic interactions with the detector material. There is an additional systematic uncertainty on the tracking efficiency from the method [24], which amounts to 0.4% (0.8%) at 7 TeV (13 TeV). For the uncertainty from the PID efficiency, the binning effect is studied by enlarging or decreasing the number of bins by a factor of two in the calculation of the PID efficiency, and taking the largest deviation from the default as the uncertainty. An additional uncertainty on the trigger efficiency is determined by testing the procedure in simulation and taking the deviation as the systematic uncertainty.

The GEC efficiency is obtained from data, and the inefficiency of the global event cuts is taken as a systematic uncertainty. The uncertainty on the offline event selection efficiencies are estimated from data and simulation by varying the selection criteria, comparing the ratios of the selection and reconstruction efficiencies between data and simulation, and taking the largest deviation as the systematic uncertainty.

A weighting procedure is applied to the simulation sample to correct for discrepancies between data and simulation in the track multiplicities. The weighting factors of the simulated events are varied within their statistical uncertainties and the largest deviation of the measured cross-section is taken as a systematic uncertainty.

5 Results

The measured B^\pm meson production cross-sections for the 7 TeV and 13 TeV data in the range $0 < p_T < 40 \text{ GeV}/c$ and $2.0 < y < 4.5$ are

$$\begin{aligned}\sigma(pp \rightarrow B^\pm X, \sqrt{s} = 7 \text{ TeV}) &= 43.0 \pm 0.2 \pm 2.5 \pm 1.7 \mu\text{b}, \\ \sigma(pp \rightarrow B^\pm X, \sqrt{s} = 13 \text{ TeV}) &= 86.6 \pm 0.5 \pm 5.4 \pm 3.4 \mu\text{b},\end{aligned}$$

where the first uncertainties are statistical, the second are systematic, and the third are due to the limited knowledge of the $B^\pm \rightarrow J/\psi K^\pm$ branching fraction.

The measured double-differential cross-sections at 7 TeV and 13 TeV as functions of p_T and y are shown in Fig. 2, where the measurements are compared with theoretical predictions based on FONLL calculations [27]. The predictions depend on assumptions

on the b -quark mass, the renormalization and factorization scales, and parton distribution functions (PDFs). The b -quark production cross-section calculated with the FONLL approach uses a b -quark mass of $4.75 \text{ GeV}/c^2$, the renormalization and factorization scales, μ_R , μ_F , set to $\mu_R = \mu_F = \mu_0 = \sqrt{m_Q^2 + p_T^2}$, where m_Q and p_T are the mass and transverse momenta of the b quark, and the CTEQ6.6 [28] PDFs. Varying the b -quark mass by $\pm 0.25 \text{ GeV}/c^2$, the μ_R/μ_F ratio by a factor of two, or using different PDFs introduces an uncertainty in the predicted b -quark production cross-section of up to 50% at low p_T [27].

The corresponding single-differential cross-sections are shown in Figs. 3 and 4. The single-differential cross-sections and the production cross-section in the above range of p_T and y are calculated from the measured double-differential cross-sections. All results are in agreement with the FONLL predictions. The results are tabulated in Appendix C.

The ratio of the cross-section at 13 TeV to that at 7 TeV, $R(13 \text{ TeV}/7 \text{ TeV})$, is determined to be

$$R(13 \text{ TeV}/7 \text{ TeV}) = 2.02 \pm 0.02 \text{ (stat)} \pm 0.12 \text{ (syst)}.$$

In the ratio calculation, the systematic uncertainties on the luminosities at 13 and 7 TeV are taken to be 50% correlated, as in Ref. [25]; the systematic uncertainties associated with the branching fractions, mass fits, event selection and binning are assumed to be completely correlated; and all other uncertainties are considered to be uncorrelated. The systematic uncertainty on R is summarised in Table 1. In Fig. 5, the ratio of the cross-section at 13 TeV to that at 7 TeV as a function of p_T or y is compared with the FONLL predictions. The measured results agree with the FONLL predictions in both the shape and the scale.

6 Summary

In summary, the double-differential production cross-sections of B^\pm mesons are measured as functions of the transverse momentum and rapidity, using pp collision data collected with the LHCb detector at the Large Hadron Collider. The integrated luminosities of the data samples are 1.0 fb^{-1} and 0.3 fb^{-1} at the centre-of-mass energies of 7 TeV and 13 TeV, respectively. The measurements are performed in the transverse momentum range $0 < p_T < 40 \text{ GeV}/c$ and the rapidity range $2.0 < y < 4.5$. The 7 TeV results are consistent with previously published results [7, 8], with improved precision in the low y region. This measurement supersedes previous results. The ratio of the production cross-section at 13 TeV to that at 7 TeV is also measured. All results are in agreement with theoretical calculations based on the FONLL approach.

Acknowledgements

We express our gratitude to our colleagues in the CERN accelerator departments for the excellent performance of the LHC. We thank the technical and administrative staff at the LHCb institutes. We acknowledge support from CERN and from the national agencies: CAPES, CNPq, FAPERJ and FINEP (Brazil); MOST and NSFC (China); CNRS/IN2P3 (France); BMBF, DFG and MPG (Germany); INFN (Italy); NWO (The Netherlands); MNiSW and NCN (Poland); MEN/IFA (Romania); MinES and FASO (Russia); MinECo

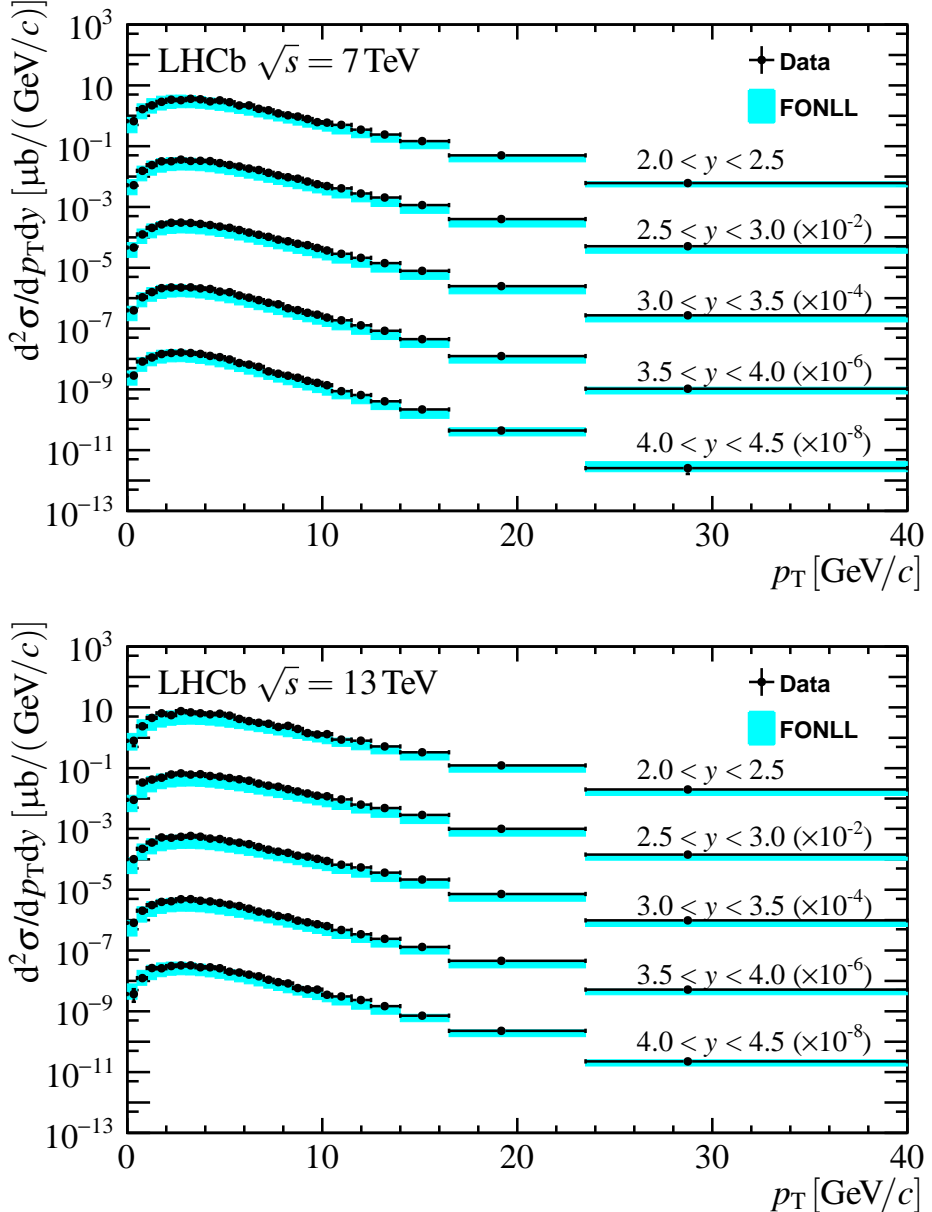


Figure 2: Measured B^\pm double-differential production cross-sections at (top) 7 TeV and (bottom) 13 TeV as a function of p_T and y . The black points represent the measured values, and the cyan bands are the FONLL predictions [27]. Each set of measurements and predictions in a given rapidity bin is offset by a multiplicative factor 10^{-m} , where the offset factor is shown after the rapidity range. The error bars include both the statistical and systematic uncertainties.

(Spain); SNSF and SER (Switzerland); NASU (Ukraine); STFC (United Kingdom); NSF (USA). We acknowledge the computing resources that are provided by CERN, IN2P3 (France), KIT and DESY (Germany), INFN (Italy), SURF (The Netherlands), PIC (Spain), GridPP (United Kingdom), RRCKI and Yandex LLC (Russia), CSCS (Switzerland), IFIN-HH (Romania), CBPF (Brazil), PL-GRID (Poland) and OSC (USA). We are indebted to the communities behind the multiple open-source software packages on which we depend. Individual groups or members have received support from AvH Foundation (Germany),

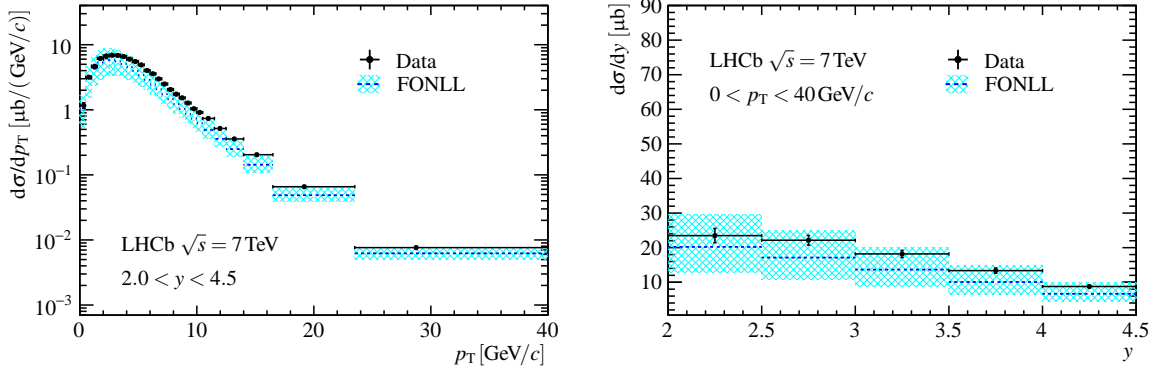


Figure 3: Measured B^\pm differential cross-section at 7 TeV as a function of (left) p_T or (right) y . The black points represent the measured values, the blue-dashed line and cyan band represent the central values and uncertainties of the FONLL prediction [27]. The error bars include both the statistical and systematic uncertainties.

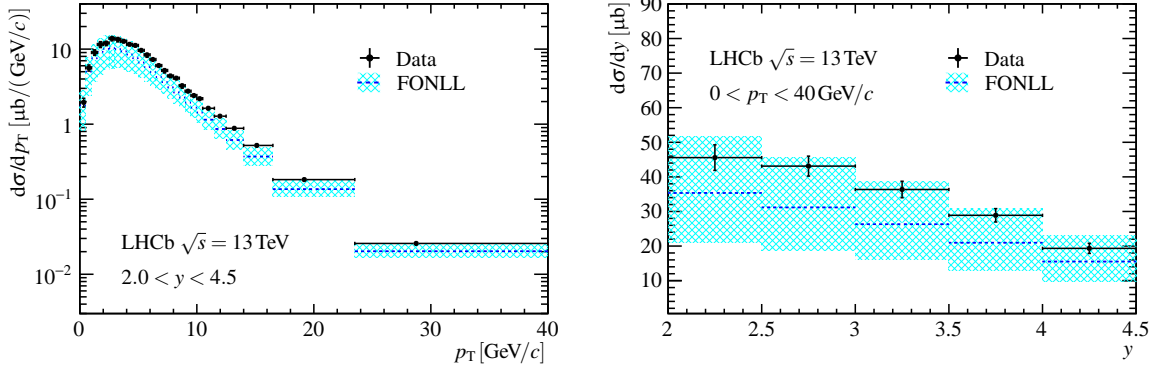


Figure 4: Measured B^\pm differential cross-section at 13 TeV as a function of (left) p_T or (right) y . The black points represent the measured values, the blue-dashed line and cyan band represent the central values and uncertainties of the FONLL prediction [27]. The error bars include both the statistical and systematic uncertainties.

EPLANET, Marie Skłodowska-Curie Actions and ERC (European Union), ANR, Labex P2IO, ENIGMASS and OCEVU, and Région Auvergne-Rhône-Alpes (France), RFBR and Yandex LLC (Russia), GVA, XuntaGal and GENCAT (Spain), Herchel Smith Fund, the Royal Society, the English-Speaking Union and the Leverhulme Trust (United Kingdom).

A Acceptance efficiency

The measured ε_{acc} as a function of p_T in different y regions are shown in Fig. 6 for 7 TeV and 13 TeV, respectively.

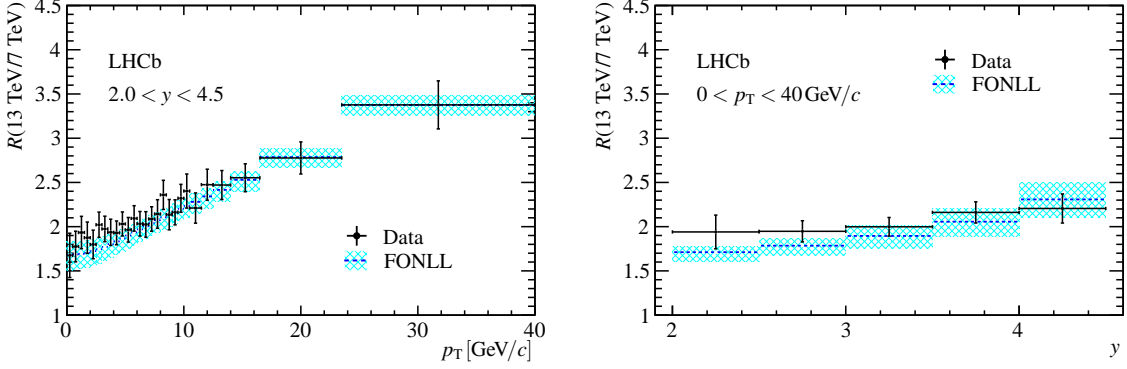


Figure 5: Ratio of the B^\pm cross-section at 13 TeV to that at 7 TeV as a function of (left) p_T or (right) y . The black points represent the measured values, the blue-dashed line and cyan band represent the central values and uncertainties of the FONLL prediction [27].

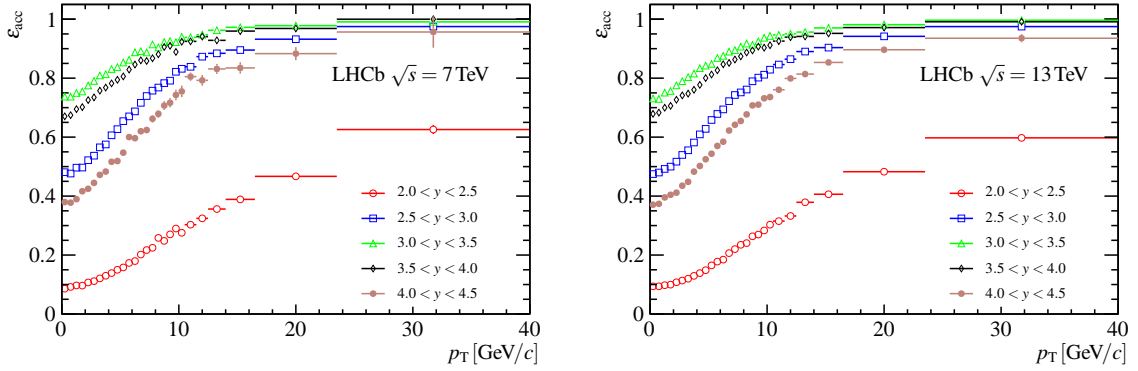


Figure 6: Measured acceptance efficiency of B^\pm events at (left) 7 TeV and (right) 13 TeV as a function of p_T in different y regions.

B Total efficiencies

The measured ε_{tot} with its statistical uncertainty as a function of p_T and y are given in Tables 2 and 3, for 7 TeV and 13 TeV, respectively. The ε_{tot} in the low p_T region are smaller than that of the high p_T region, due to the lifetime cut effects. Also with limited detector coverage, ε_{tot} in the boundary regions ($2.0 < y < 2.5$ and $4.0 < y < 4.5$) are smaller than that in central regions.

C Tabulated results

The measured B^\pm double-differential cross-section in bins of p_T and y is given in Tables 4 and 5 for 7 TeV data, and Tables 6 and 7 for 13 TeV data. The measured B^\pm single-differential cross-section as a function of p_T or y is given in Tables 8 and 9, respectively. The limited size of the simulation samples gives relative systematic uncertainties in the high p_T region that are larger than those in the low p_T region.

Table 2: Measured ε_{tot} of B^\pm events at 7 TeV, in the bins of $B^\pm p_T$ and y . The efficiencies and uncertainties are in percent.

p_T [GeV/c]		$2.0 < y < 2.5$	$2.5 < y < 3.0$	$3.0 < y < 3.5$	$3.5 < y < 4.0$	$4.0 < y < 4.5$
0.0 – 0.5		0.6±0.1	5.4±0.3	10.6±0.5	9.4±0.5	4.0±0.3
0.5 – 1.0		0.7±0.0	5.3±0.2	10.3±0.4	10.0±0.5	4.2±0.3
1.0 – 1.5		0.8±0.0	5.7±0.2	10.4±0.4	10.6±0.4	4.4±0.2
1.5 – 2.0		0.8±0.0	6.1±0.2	10.8±0.4	10.8±0.4	4.8±0.3
2.0 – 2.5		0.9±0.0	6.7±0.2	11.6±0.4	11.4±0.5	5.0±0.3
2.5 – 3.0		1.0±0.0	7.2±0.3	12.3±0.4	12.1±0.5	5.6±0.3
3.0 – 3.5		1.1±0.1	7.9±0.3	13.3±0.5	12.7±0.5	5.8±0.3
3.5 – 4.0		1.2±0.1	8.3±0.3	13.8±0.4	13.3±0.5	5.7±0.3
4.0 – 4.5		1.4±0.1	8.8±0.3	14.6±0.5	14.0±0.5	6.2±0.3
4.5 – 5.0		1.6±0.1	10.0±0.3	15.4±0.4	14.7±0.5	6.4±0.3
5.0 – 5.5		1.6±0.1	10.6±0.3	16.0±0.4	14.9±0.5	6.9±0.3
5.5 – 6.0		2.0±0.1	11.4±0.3	16.8±0.5	15.9±0.5	7.9±0.4
6.0 – 6.5		2.2±0.1	12.3±0.3	17.8±0.5	16.7±0.5	7.8±0.4
6.5 – 7.0		2.6±0.1	13.0±0.3	18.8±0.5	17.1±0.5	8.2±0.4
7.0 – 7.5		3.0±0.1	14.2±0.3	19.2±0.4	17.7±0.5	9.0±0.4
7.5 – 8.0		3.3±0.1	15.0±0.3	20.9±0.4	18.4±0.4	9.0±0.4
8.0 – 8.5		3.9±0.1	16.5±0.3	21.1±0.3	20.6±0.4	9.6±0.4
8.5 – 9.0		4.2±0.1	17.1±0.3	21.7±0.3	21.1±0.4	10.2±0.4
9.0 – 9.5		4.5±0.2	17.9±0.3	23.2±0.3	21.2±0.4	11.5±0.5
9.5 – 10.0		5.3±0.2	19.4±0.3	24.0±0.4	21.6±0.5	12.1±0.5
10.0 – 10.5		5.2±0.2	20.3±0.4	24.7±0.4	22.9±0.5	11.9±0.6
10.5 – 11.5		6.0±0.2	21.3±0.3	25.9±0.3	24.2±0.4	13.8±0.5
11.5 – 12.5		7.0±0.2	23.5±0.3	26.8±0.4	26.1±0.5	15.3±0.7
12.5 – 14.0		8.4±0.2	24.4±0.3	27.9±0.4	26.2±0.5	15.2±0.7
14.0 – 16.5		9.9±0.3	26.3±0.4	29.1±0.4	27.4±0.6	16.6±0.8
16.5 – 23.5		13.2±0.3	28.4±0.4	30.3±0.4	29.8±0.7	19.3±1.0
23.5 – 40.0		18.9±0.7	30.6±0.7	31.0±0.9	28.0±1.6	18.0±3.1

Table 3: Measured ε_{tot} of B^\pm events at 13 TeV, in the bins of $B^\pm p_T$ and y . The efficiencies and uncertainties are in percent.

p_T [GeV/c]		$2.0 < y < 2.5$	$2.5 < y < 3.0$	$3.0 < y < 3.5$	$3.5 < y < 4.0$	$4.0 < y < 4.5$
0.0 – 0.5		0.8±0.1	4.7±0.1	7.6±0.2	6.8±0.2	2.3±0.1
0.5 – 1.0		0.8±0.0	4.9±0.1	7.8±0.1	7.0±0.1	2.6±0.1
1.0 – 1.5		0.8±0.0	5.4±0.1	8.4±0.1	7.3±0.1	2.7±0.1
1.5 – 2.0		0.9±0.0	5.5±0.1	8.6±0.1	7.5±0.1	2.9±0.1
2.0 – 2.5		0.9±0.0	6.1±0.1	9.6±0.1	8.2±0.1	3.1±0.1
2.5 – 3.0		1.0±0.0	6.6±0.1	10.1±0.1	8.7±0.1	3.4±0.1
3.0 – 3.5		1.2±0.0	7.0±0.1	10.5±0.1	9.2±0.1	3.5±0.1
3.5 – 4.0		1.3±0.0	7.7±0.1	11.3±0.2	9.6±0.2	3.8±0.1
4.0 – 4.5		1.4±0.0	8.3±0.1	11.8±0.2	9.9±0.2	4.0±0.1
4.5 – 5.0		1.6±0.0	8.7±0.1	12.4±0.2	10.6±0.2	4.3±0.1
5.0 – 5.5		1.8±0.0	9.7±0.1	13.0±0.1	11.1±0.1	4.4±0.1
5.5 – 6.0		2.1±0.1	10.3±0.1	14.0±0.2	11.7±0.2	4.9±0.1
6.0 – 6.5		2.3±0.1	11.1±0.1	14.6±0.2	12.3±0.2	5.1±0.1
6.5 – 7.0		2.6±0.1	12.0±0.2	14.9±0.2	13.0±0.2	5.4±0.1
7.0 – 7.5		3.0±0.1	13.0±0.2	15.6±0.2	13.4±0.2	5.9±0.2
7.5 – 8.0		3.2±0.1	13.3±0.2	16.8±0.2	14.4±0.2	6.3±0.2
8.0 – 8.5		3.5±0.1	14.3±0.2	17.2±0.2	15.0±0.3	6.6±0.2
8.5 – 9.0		4.0±0.1	15.3±0.2	18.0±0.2	16.0±0.3	7.0±0.2
9.0 – 9.5		4.4±0.1	16.2±0.2	18.9±0.3	16.8±0.3	7.7±0.3
9.5 – 10.0		5.2±0.2	17.8±0.3	19.8±0.3	17.4±0.3	7.7±0.3
10.0 – 10.5		5.8±0.2	18.2±0.3	20.4±0.3	18.3±0.4	8.4±0.3
10.5 – 11.5		6.3±0.2	19.0±0.2	21.5±0.3	18.9±0.3	9.1±0.3
11.5 – 12.5		7.1±0.2	20.5±0.3	22.0±0.3	21.0±0.4	9.7±0.3
12.5 – 14.0		8.7±0.2	22.7±0.3	23.6±0.3	21.0±0.4	10.7±0.3
14.0 – 16.5		10.5±0.2	24.3±0.3	24.6±0.3	22.5±0.4	11.7±0.4
16.5 – 23.5		13.4±0.2	27.0±0.3	26.2±0.3	24.1±0.4	13.0±0.4
23.5 – 40.0		18.2±0.5	29.0±0.5	26.9±0.6	24.0±0.8	14.0±1.0

Table 4: Measured B^\pm double-differential cross-section (in units of nb) at 7 TeV, as a function of p_T and y , in the rapidity regions of $2.0 < y < 2.5$, $2.5 < y < 3.0$, and $3.0 < y < 3.5$.

p_T [GeV/c]		$2.0 < y < 2.5$	$2.5 < y < 3.0$	$3.0 < y < 3.5$
0.0 – 0.5		$664.5 \pm 103.3 \pm 99.9$	$519.8 \pm 35.0 \pm 50.3$	$462.6 \pm 30.4 \pm 37.5$
0.5 – 1.0		$1652.9 \pm 160.9 \pm 180.6$	$1544.9 \pm 59.8 \pm 142.0$	$1248.8 \pm 51.6 \pm 94.4$
1.0 – 1.5		$2204.8 \pm 171.7 \pm 345.8$	$2381.1 \pm 71.0 \pm 212.8$	$2046.2 \pm 62.4 \pm 147.1$
1.5 – 2.0		$2879.5 \pm 191.3 \pm 311.6$	$3175.6 \pm 76.2 \pm 260.1$	$2665.7 \pm 65.1 \pm 192.5$
2.0 – 2.5		$3378.9 \pm 192.0 \pm 592.5$	$3193.0 \pm 80.1 \pm 257.7$	$3017.2 \pm 64.1 \pm 214.6$
2.5 – 3.0		$3261.7 \pm 179.8 \pm 321.9$	$3605.8 \pm 69.9 \pm 256.6$	$3056.6 \pm 60.7 \pm 220.0$
3.0 – 3.5		$3627.8 \pm 182.8 \pm 290.3$	$3263.8 \pm 66.6 \pm 263.4$	$2977.6 \pm 54.6 \pm 194.2$
3.5 – 4.0		$3491.7 \pm 175.6 \pm 419.5$	$3304.0 \pm 57.9 \pm 246.3$	$2767.2 \pm 49.8 \pm 167.7$
4.0 – 4.5		$2976.6 \pm 146.4 \pm 240.0$	$3224.0 \pm 50.9 \pm 233.4$	$2545.6 \pm 44.7 \pm 173.3$
4.5 – 5.0		$3216.9 \pm 141.1 \pm 255.9$	$2773.2 \pm 44.1 \pm 185.0$	$2258.6 \pm 39.7 \pm 134.8$
5.0 – 5.5		$2795.0 \pm 127.6 \pm 308.6$	$2408.0 \pm 41.3 \pm 158.0$	$2063.8 \pm 36.1 \pm 128.5$
5.5 – 6.0		$2183.8 \pm 101.3 \pm 160.2$	$2145.3 \pm 34.4 \pm 136.9$	$1740.5 \pm 31.3 \pm 108.4$
6.0 – 6.5		$2194.2 \pm 94.8 \pm 200.1$	$1834.6 \pm 28.8 \pm 124.7$	$1437.9 \pm 27.3 \pm 85.9$
6.5 – 7.0		$1694.1 \pm 75.0 \pm 166.0$	$1645.1 \pm 24.4 \pm 109.0$	$1219.0 \pm 23.7 \pm 69.7$
7.0 – 7.5		$1517.7 \pm 65.6 \pm 102.6$	$1329.8 \pm 21.9 \pm 84.9$	$1039.8 \pm 21.4 \pm 59.3$
7.5 – 8.0		$1200.0 \pm 54.2 \pm 134.2$	$1101.1 \pm 18.7 \pm 73.8$	$842.3 \pm 18.1 \pm 48.4$
8.0 – 8.5		$1036.9 \pm 46.2 \pm 91.2$	$950.4 \pm 16.7 \pm 55.4$	$744.6 \pm 16.7 \pm 41.3$
8.5 – 9.0		$943.1 \pm 42.4 \pm 124.1$	$851.6 \pm 14.1 \pm 50.5$	$614.3 \pm 14.9 \pm 33.3$
9.0 – 9.5		$782.0 \pm 36.7 \pm 57.8$	$687.3 \pm 13.9 \pm 39.6$	$554.8 \pm 13.5 \pm 30.0$
9.5 – 10.0		$617.0 \pm 30.0 \pm 49.2$	$559.9 \pm 11.9 \pm 32.8$	$448.5 \pm 11.9 \pm 27.1$
10.0 – 10.5		$594.6 \pm 29.4 \pm 79.9$	$487.7 \pm 10.2 \pm 26.9$	$371.0 \pm 10.7 \pm 21.6$
10.5 – 11.5		$502.1 \pm 17.6 \pm 55.1$	$409.9 \pm 5.9 \pm 25.7$	$287.9 \pm 6.4 \pm 15.3$
11.5 – 12.5		$349.3 \pm 13.5 \pm 38.7$	$278.0 \pm 5.0 \pm 14.7$	$212.3 \pm 5.4 \pm 11.6$
12.5 – 14.0		$241.5 \pm 8.4 \pm 20.0$	$204.5 \pm 3.1 \pm 11.5$	$142.1 \pm 3.5 \pm 9.9$
14.0 – 16.5		$146.9 \pm 4.6 \pm 9.2$	$115.4 \pm 1.7 \pm 6.3$	$79.2 \pm 2.0 \pm 6.5$
16.5 – 23.5		$49.9 \pm 1.4 \pm 2.9$	$40.0 \pm 0.5 \pm 2.9$	$24.8 \pm 0.6 \pm 1.9$
23.5 – 40.0		$6.1 \pm 0.3 \pm 0.4$	$5.1 \pm 0.1 \pm 0.4$	$2.7 \pm 0.1 \pm 0.3$

Table 5: Measured B^\pm double-differential cross-section (in units of nb) at 7 TeV, as a function of p_T and y , in the rapidity regions of $3.5 < y < 4.0$ and $4.0 < y < 4.5$.

p_T (GeV/c)		$3.5 < y < 4.0$	$4.0 < y < 4.5$
0.0 – 0.5		$396.4 \pm 29.2 \pm 34.4$	$283.7 \pm 37.9 \pm 35.3$
0.5 – 1.0		$1069.6 \pm 43.9 \pm 83.6$	$820.5 \pm 57.0 \pm 83.9$
1.0 – 1.5		$1581.2 \pm 50.0 \pm 121.1$	$1115.7 \pm 63.6 \pm 102.2$
1.5 – 2.0		$2132.1 \pm 53.8 \pm 161.0$	$1447.6 \pm 65.7 \pm 146.7$
2.0 – 2.5		$2256.6 \pm 52.1 \pm 165.1$	$1570.9 \pm 63.2 \pm 145.3$
2.5 – 3.0		$2241.9 \pm 48.6 \pm 158.9$	$1627.4 \pm 58.5 \pm 133.5$
3.0 – 3.5		$2265.2 \pm 45.6 \pm 157.5$	$1566.6 \pm 55.1 \pm 134.3$
3.5 – 4.0		$2094.9 \pm 42.2 \pm 147.0$	$1465.1 \pm 52.1 \pm 113.5$
4.0 – 4.5		$2002.0 \pm 39.2 \pm 133.4$	$1259.9 \pm 45.5 \pm 114.5$
4.5 – 5.0		$1642.0 \pm 34.0 \pm 101.1$	$1144.0 \pm 42.8 \pm 101.4$
5.0 – 5.5		$1569.5 \pm 32.0 \pm 108.9$	$961.9 \pm 37.0 \pm 76.5$
5.5 – 6.0		$1223.2 \pm 27.2 \pm 75.1$	$734.2 \pm 29.8 \pm 73.7$
6.0 – 6.5		$1038.0 \pm 23.7 \pm 62.5$	$652.5 \pm 27.6 \pm 48.4$
6.5 – 7.0		$861.0 \pm 20.8 \pm 53.3$	$548.6 \pm 24.1 \pm 44.0$
7.0 – 7.5		$704.6 \pm 18.2 \pm 40.9$	$390.1 \pm 19.2 \pm 28.5$
7.5 – 8.0		$628.7 \pm 16.6 \pm 37.2$	$326.4 \pm 17.4 \pm 27.7$
8.0 – 8.5		$465.3 \pm 13.4 \pm 28.3$	$280.7 \pm 15.3 \pm 21.2$
8.5 – 9.0		$403.4 \pm 12.2 \pm 22.3$	$241.0 \pm 13.5 \pm 17.7$
9.0 – 9.5		$330.0 \pm 11.0 \pm 20.8$	$190.6 \pm 11.4 \pm 17.6$
9.5 – 10.0		$286.9 \pm 10.2 \pm 17.7$	$163.9 \pm 10.2 \pm 14.2$
10.0 – 10.5		$230.0 \pm 8.8 \pm 13.8$	$136.7 \pm 9.5 \pm 15.3$
10.5 – 11.5		$186.7 \pm 5.4 \pm 10.5$	$87.0 \pm 4.9 \pm 8.2$
11.5 – 12.5		$127.7 \pm 4.3 \pm 7.3$	$65.0 \pm 4.0 \pm 5.5$
12.5 – 14.0		$84.4 \pm 2.8 \pm 4.8$	$40.4 \pm 2.6 \pm 3.5$
14.0 – 16.5		$44.7 \pm 1.6 \pm 2.7$	$21.8 \pm 1.4 \pm 1.8$
16.5 – 23.5		$12.4 \pm 0.5 \pm 0.8$	$4.4 \pm 0.3 \pm 0.4$
23.5 – 40.0		$1.0 \pm 0.1 \pm 0.1$	$0.3 \pm 0.1 \pm 0.1$

Table 6: Measured B^\pm double-differential cross-section (in units of nb) at 13 TeV, as a function of p_T and y , in the rapidity regions of $2.0 < y < 2.5$, $2.5 < y < 3.0$, and $3.0 < y < 3.5$.

p_T [GeV/c]		$2.0 < y < 2.5$	$2.5 < y < 3.0$	$3.0 < y < 3.5$
0.0 – 0.5		$794.4 \pm 228.1 \pm 130.0$	$905.7 \pm 152.4 \pm 85.6$	$1013.9 \pm 183.2 \pm 81.1$
0.5 – 1.0		$2384.0 \pm 362.6 \pm 322.3$	$3371.6 \pm 178.9 \pm 267.2$	$2221.2 \pm 194.6 \pm 152.5$
1.0 – 1.5		$4503.0 \pm 493.3 \pm 419.1$	$4211.5 \pm 232.8 \pm 321.1$	$3557.8 \pm 223.2 \pm 236.1$
1.5 – 2.0		$6378.3 \pm 557.8 \pm 939.8$	$4846.7 \pm 297.1 \pm 356.4$	$5255.5 \pm 236.4 \pm 370.7$
2.0 – 2.5		$5543.9 \pm 518.5 \pm 501.1$	$6186.6 \pm 236.4 \pm 465.9$	$5136.2 \pm 214.9 \pm 347.9$
2.5 – 3.0		$7517.2 \pm 555.3 \pm 695.2$	$6739.7 \pm 217.1 \pm 477.0$	$5519.8 \pm 203.8 \pm 369.2$
3.0 – 3.5		$6848.8 \pm 534.6 \pm 738.4$	$6152.6 \pm 228.5 \pm 412.6$	$5903.7 \pm 189.0 \pm 419.3$
3.5 – 4.0		$6382.6 \pm 475.5 \pm 509.5$	$6321.5 \pm 187.5 \pm 452.4$	$5560.9 \pm 167.3 \pm 368.1$
4.0 – 4.5		$5900.1 \pm 449.8 \pm 543.6$	$5525.8 \pm 162.8 \pm 371.3$	$4824.6 \pm 144.4 \pm 315.7$
4.5 – 5.0		$6185.4 \pm 412.5 \pm 503.8$	$5259.5 \pm 150.0 \pm 368.0$	$4657.9 \pm 131.8 \pm 318.8$
5.0 – 5.5		$5353.0 \pm 349.5 \pm 402.2$	$4735.5 \pm 119.4 \pm 313.3$	$3900.2 \pm 113.6 \pm 256.2$
5.5 – 6.0		$4168.6 \pm 279.7 \pm 357.4$	$4300.4 \pm 105.7 \pm 290.2$	$3535.4 \pm 101.0 \pm 245.1$
6.0 – 6.5		$3532.0 \pm 237.5 \pm 326.4$	$3865.7 \pm 92.1 \pm 256.5$	$3158.4 \pm 88.8 \pm 211.9$
6.5 – 7.0		$3111.7 \pm 203.9 \pm 259.2$	$3107.7 \pm 77.0 \pm 227.6$	$2544.5 \pm 77.0 \pm 167.0$
7.0 – 7.5		$2891.4 \pm 174.3 \pm 282.1$	$2662.1 \pm 63.4 \pm 177.2$	$2086.4 \pm 66.5 \pm 143.7$
7.5 – 8.0		$2270.4 \pm 149.5 \pm 182.8$	$2450.3 \pm 54.9 \pm 164.1$	$1788.4 \pm 58.2 \pm 122.9$
8.0 – 8.5		$2467.8 \pm 143.9 \pm 213.3$	$2034.0 \pm 52.1 \pm 149.6$	$1638.5 \pm 53.4 \pm 109.7$
8.5 – 9.0		$1947.3 \pm 118.9 \pm 195.0$	$1710.1 \pm 44.0 \pm 118.7$	$1320.5 \pm 46.2 \pm 87.5$
9.0 – 9.5		$1424.4 \pm 98.0 \pm 115.2$	$1472.0 \pm 41.9 \pm 99.1$	$1227.2 \pm 42.8 \pm 83.0$
9.5 – 10.0		$1283.7 \pm 84.4 \pm 96.4$	$1243.8 \pm 36.7 \pm 86.2$	$1039.0 \pm 38.0 \pm 74.6$
10.0 – 10.5		$1313.6 \pm 78.7 \pm 100.9$	$1189.3 \pm 31.3 \pm 79.5$	$883.8 \pm 34.3 \pm 59.3$
10.5 – 11.5		$870.5 \pm 43.3 \pm 67.7$	$936.9 \pm 18.1 \pm 68.1$	$666.8 \pm 20.5 \pm 44.4$
11.5 – 12.5		$802.2 \pm 38.1 \pm 66.1$	$632.3 \pm 17.1 \pm 42.4$	$541.7 \pm 17.9 \pm 36.4$
12.5 – 14.0		$518.5 \pm 22.4 \pm 36.2$	$487.1 \pm 10.1 \pm 32.1$	$365.3 \pm 11.6 \pm 24.7$
14.0 – 16.5		$333.0 \pm 12.5 \pm 23.2$	$289.2 \pm 5.8 \pm 19.6$	$216.4 \pm 6.7 \pm 14.3$
16.5 – 23.5		$123.1 \pm 4.0 \pm 9.3$	$101.0 \pm 1.8 \pm 6.6$	$72.4 \pm 2.2 \pm 5.1$
23.5 – 40.0		$19.9 \pm 0.9 \pm 1.4$	$14.3 \pm 0.4 \pm 1.1$	$9.8 \pm 0.5 \pm 0.7$

Table 7: Measured B^\pm double-differential cross-section (in units of nb) at 13 TeV, as a function of p_T and y , in the rapidity regions of $3.5 < y < 4.0$ and $4.0 < y < 4.5$.

p_T (GeV/c)		$3.5 < y < 4.0$	$4.0 < y < 4.5$
0.0 – 0.5		$814.7 \pm 111.2 \pm 83.4$	$369.7 \pm 156.1 \pm 48.4$
0.5 – 1.0		$2037.6 \pm 161.1 \pm 165.9$	$1235.7 \pm 197.9 \pm 107.4$
1.0 – 1.5		$3120.6 \pm 186.1 \pm 288.9$	$2649.3 \pm 249.5 \pm 236.6$
1.5 – 2.0		$3980.7 \pm 202.0 \pm 266.5$	$2605.7 \pm 236.3 \pm 238.8$
2.0 – 2.5		$4187.1 \pm 185.7 \pm 288.7$	$3079.7 \pm 240.3 \pm 232.1$
2.5 – 3.0		$4869.2 \pm 179.4 \pm 332.8$	$3237.0 \pm 224.2 \pm 252.6$
3.0 – 3.5		$4898.3 \pm 168.1 \pm 327.0$	$3246.0 \pm 210.9 \pm 257.8$
3.5 – 4.0		$4336.9 \pm 149.4 \pm 343.3$	$2807.4 \pm 185.1 \pm 268.8$
4.0 – 4.5		$4118.0 \pm 140.2 \pm 283.3$	$2804.3 \pm 171.0 \pm 225.4$
4.5 – 5.0		$3690.8 \pm 121.8 \pm 249.0$	$2611.4 \pm 153.9 \pm 187.4$
5.0 – 5.5		$3248.0 \pm 108.5 \pm 213.2$	$2013.2 \pm 133.7 \pm 151.5$
5.5 – 6.0		$2910.9 \pm 96.5 \pm 193.3$	$1886.3 \pm 123.0 \pm 207.7$
6.0 – 6.5		$2381.8 \pm 83.6 \pm 157.1$	$1610.8 \pm 105.5 \pm 129.0$
6.5 – 7.0		$1907.1 \pm 70.2 \pm 126.9$	$1415.9 \pm 93.2 \pm 112.7$
7.0 – 7.5		$1661.2 \pm 63.4 \pm 119.0$	$1095.4 \pm 76.5 \pm 83.1$
7.5 – 8.0		$1364.5 \pm 54.1 \pm 96.8$	$910.1 \pm 66.1 \pm 74.4$
8.0 – 8.5		$1238.8 \pm 49.7 \pm 83.7$	$826.1 \pm 60.3 \pm 63.9$
8.5 – 9.0		$961.2 \pm 41.8 \pm 64.3$	$581.5 \pm 50.7 \pm 50.9$
9.0 – 9.5		$848.9 \pm 38.4 \pm 57.0$	$528.5 \pm 44.7 \pm 43.7$
9.5 – 10.0		$732.8 \pm 34.6 \pm 50.4$	$518.6 \pm 43.0 \pm 43.7$
10.0 – 10.5		$635.7 \pm 30.9 \pm 60.2$	$350.2 \pm 33.9 \pm 32.1$
10.5 – 11.5		$474.4 \pm 18.4 \pm 33.1$	$308.7 \pm 21.6 \pm 25.2$
11.5 – 12.5		$343.0 \pm 14.7 \pm 24.8$	$235.5 \pm 18.0 \pm 19.1$
12.5 – 14.0		$242.6 \pm 10.2 \pm 16.3$	$147.9 \pm 11.1 \pm 13.1$
14.0 – 16.5		$131.0 \pm 5.6 \pm 8.8$	$71.8 \pm 5.7 \pm 5.7$
16.5 – 23.5		$45.9 \pm 1.9 \pm 3.2$	$22.8 \pm 1.9 \pm 2.0$
23.5 – 40.0		$5.2 \pm 0.4 \pm 0.4$	$2.3 \pm 0.4 \pm 0.3$

Table 8: Measured B^\pm differential cross-sections (in units of nb) at 7 TeV and 13 TeV as functions of p_T in the range $2.0 < y < 4.5$. The cross-section ratio between 13 TeV and 7 TeV is also presented.

p_T [GeV/c]		7 TeV	13 TeV	$R(13/7)$
0.0 – 0.5		$1163.5 \pm 62.1 \pm 101.8$	$1949.2 \pm 187.7 \pm 182.4$	$1.68 \pm 0.18 \pm 0.17$
0.5 – 1.0		$3168.4 \pm 99.0 \pm 237.0$	$5625.1 \pm 277.6 \pm 444.3$	$1.78 \pm 0.10 \pm 0.14$
1.0 – 1.5		$4664.6 \pm 108.1 \pm 383.1$	$9021.1 \pm 341.3 \pm 676.1$	$1.93 \pm 0.09 \pm 0.16$
1.5 – 2.0		$6150.2 \pm 118.6 \pm 459.3$	$11533.4 \pm 367.0 \pm 972.4$	$1.88 \pm 0.07 \pm 0.16$
2.0 – 2.5		$6708.3 \pm 117.1 \pm 566.0$	$12066.8 \pm 349.4 \pm 856.8$	$1.80 \pm 0.06 \pm 0.15$
2.5 – 3.0		$6896.7 \pm 110.2 \pm 454.0$	$13941.5 \pm 354.5 \pm 978.2$	$2.02 \pm 0.06 \pm 0.13$
3.0 – 3.5		$6850.5 \pm 108.2 \pm 442.2$	$13524.7 \pm 335.7 \pm 981.9$	$1.97 \pm 0.06 \pm 0.13$
3.5 – 4.0		$6561.5 \pm 103.2 \pm 462.6$	$12704.7 \pm 298.4 \pm 881.2$	$1.94 \pm 0.05 \pm 0.14$
4.0 – 4.5		$6004.1 \pm 88.3 \pm 388.6$	$11586.5 \pm 277.0 \pm 794.5$	$1.93 \pm 0.05 \pm 0.12$
4.5 – 5.0		$5517.3 \pm 82.8 \pm 338.2$	$11202.5 \pm 252.3 \pm 761.9$	$2.03 \pm 0.05 \pm 0.12$
5.0 – 5.5		$4899.1 \pm 74.7 \pm 335.9$	$9625.0 \pm 215.4 \pm 628.0$	$1.96 \pm 0.05 \pm 0.13$
5.5 – 6.0		$4013.5 \pm 60.5 \pm 238.5$	$8400.8 \pm 179.9 \pm 594.3$	$2.09 \pm 0.05 \pm 0.13$
6.0 – 6.5		$3578.6 \pm 55.7 \pm 222.7$	$7274.4 \pm 154.2 \pm 494.3$	$2.03 \pm 0.05 \pm 0.13$
6.5 – 7.0		$2983.9 \pm 45.5 \pm 189.6$	$6043.4 \pm 132.2 \pm 415.3$	$2.03 \pm 0.05 \pm 0.13$
7.0 – 7.5		$2491.0 \pm 39.5 \pm 137.1$	$5198.3 \pm 113.2 \pm 369.3$	$2.09 \pm 0.06 \pm 0.13$
7.5 – 8.0		$2049.2 \pm 33.3 \pm 141.3$	$4391.8 \pm 98.3 \pm 297.9$	$2.14 \pm 0.06 \pm 0.15$
8.0 – 8.5		$1738.9 \pm 28.6 \pm 104.5$	$4102.6 \pm 92.0 \pm 286.4$	$2.36 \pm 0.07 \pm 0.15$
8.5 – 9.0		$1526.7 \pm 26.2 \pm 104.5$	$3260.3 \pm 77.2 \pm 233.3$	$2.14 \pm 0.06 \pm 0.16$
9.0 – 9.5		$1272.3 \pm 22.8 \pm 73.1$	$2750.5 \pm 66.0 \pm 183.0$	$2.16 \pm 0.06 \pm 0.13$
9.5 – 10.0		$1038.1 \pm 19.2 \pm 62.6$	$2408.9 \pm 58.2 \pm 160.6$	$2.32 \pm 0.07 \pm 0.14$
10.0 – 10.5		$909.9 \pm 18.2 \pm 65.8$	$2186.3 \pm 53.0 \pm 148.1$	$2.40 \pm 0.08 \pm 0.18$
10.5 – 11.5		$736.8 \pm 10.9 \pm 51.2$	$1628.7 \pm 30.6 \pm 113.0$	$2.21 \pm 0.05 \pm 0.16$
11.5 – 12.5		$516.2 \pm 8.5 \pm 32.7$	$1277.4 \pm 26.0 \pm 87.0$	$2.47 \pm 0.06 \pm 0.16$
12.5 – 14.0		$356.5 \pm 5.4 \pm 22.3$	$880.7 \pm 16.1 \pm 57.2$	$2.47 \pm 0.06 \pm 0.15$
14.0 – 16.5		$204.0 \pm 3.0 \pm 11.8$	$520.7 \pm 9.0 \pm 33.9$	$2.55 \pm 0.06 \pm 0.15$
16.5 – 23.5		$65.8 \pm 0.9 \pm 3.9$	$182.6 \pm 2.9 \pm 12.4$	$2.78 \pm 0.06 \pm 0.17$
23.5 – 40.0		$7.6 \pm 0.2 \pm 0.6$	$25.7 \pm 0.6 \pm 1.8$	$3.38 \pm 0.12 \pm 0.25$

Table 9: Measured B^\pm differential cross-sections (in units of μb) at 7 TeV and 13 TeV as functions of y in the p_T range $0 < p_T < 40 \text{ GeV}/c$. The cross-section ratio between 13 TeV and 7 TeV is also presented.

y		7 TeV	13 TeV	$R(13/7)$
2.0 – 2.5		$23.5 \pm 0.3 \pm 2.0$	$45.6 \pm 0.8 \pm 3.6$	$1.94 \pm 0.04 \pm 0.19$
2.5 – 3.0		$22.1 \pm 0.1 \pm 1.4$	$43.1 \pm 0.4 \pm 2.9$	$1.95 \pm 0.02 \pm 0.12$
3.0 – 3.5		$18.2 \pm 0.1 \pm 1.0$	$36.4 \pm 0.3 \pm 2.4$	$2.00 \pm 0.02 \pm 0.10$
3.5 – 4.0		$13.4 \pm 0.1 \pm 0.8$	$28.9 \pm 0.3 \pm 1.9$	$2.16 \pm 0.02 \pm 0.12$
4.0 – 4.5		$8.8 \pm 0.1 \pm 0.6$	$19.3 \pm 0.4 \pm 1.4$	$2.21 \pm 0.05 \pm 0.16$

References

- [1] M. Cacciari, M. Greco, and P. Nason, *The p_T spectrum in heavy flavor hadroproduction*, JHEP **05** (1998) 007, [arXiv:hep-ph/9803400](#).
- [2] M. Cacciari, S. Frixione, and P. Nason, *The p_T spectrum in heavy flavor photoproduction*, JHEP **03** (2001) 006, [arXiv:hep-ph/0102134](#).
- [3] LHCb collaboration, R. Aaij *et al.*, *Measurement of b hadron production fractions in 7 TeV pp collisions*, Phys. Rev. **D85** (2012) 032008, [arXiv:1111.2357](#).
- [4] CMS collaboration, V. Khachatryan *et al.*, *Measurement of the B^+ production cross section in pp collisions at $\sqrt{s} = 7$ TeV*, Phys. Rev. Lett. **106** (2011) 112001, [arXiv:1101.0131](#).
- [5] CMS collaboration, V. Khachatryan *et al.*, *Measurement of the total and differential inclusive B^+ hadron cross sections in pp collisions at $\sqrt{s} = 13$ TeV*, Phys. Lett. **B771** (2017) 435, [arXiv:1609.00873](#).
- [6] ATLAS collaboration, G. Aad *et al.*, *Measurement of the differential cross-section of B^+ meson production in pp collisions at $\sqrt{s} = 7$ TeV at ATLAS*, JHEP **10** (2013) 042, [arXiv:1307.0126](#).
- [7] LHCb collaboration, R. Aaij *et al.*, *Measurement of the B^\pm production cross-section in pp collisions at $\sqrt{s} = 7$ TeV*, JHEP **04** (2012) 093, [arXiv:1202.4812](#).
- [8] LHCb collaboration, R. Aaij *et al.*, *Measurement of B meson production cross-sections in proton-proton collisions at $\sqrt{s} = 7$ TeV*, JHEP **08** (2013) 117, [arXiv:1306.3663](#).
- [9] LHCb collaboration, A. A. Alves Jr. *et al.*, *The LHCb detector at the LHC*, JINST **3** (2008) S08005.
- [10] LHCb collaboration, R. Aaij *et al.*, *LHCb detector performance*, Int. J. Mod. Phys. **A30** (2015) 1530022, [arXiv:1412.6352](#).
- [11] R. Aaij *et al.*, *The LHCb trigger and its performance in 2011*, JINST **8** (2013) P04022, [arXiv:1211.3055](#).
- [12] Particle Data Group, C. Patrignani *et al.*, *Review of particle physics*, Chin. Phys. **C40** (2016) 100001.
- [13] T. Sjöstrand, S. Mrenna, and P. Skands, *A brief introduction to PYTHIA 8.1*, Comput. Phys. Commun. **178** (2008) 852, [arXiv:0710.3820](#).
- [14] I. Belyaev *et al.*, *Handling of the generation of primary events in Gauss, the LHCb simulation framework*, J. Phys. Conf. Ser. **331** (2011) 032047.
- [15] D. J. Lange, *The EvtGen particle decay simulation package*, Nucl. Instrum. Meth. **A462** (2001) 152.
- [16] P. Golonka and Z. Was, *PHOTOS Monte Carlo: A precision tool for QED corrections in Z and W decays*, Eur. Phys. J. **C45** (2006) 97, [arXiv:hep-ph/0506026](#).

- [17] Geant4 collaboration, J. Allison *et al.*, *Geant4 developments and applications*, IEEE Trans. Nucl. Sci. **53** (2006) 270; Geant4 collaboration, S. Agostinelli *et al.*, *Geant4: A simulation toolkit*, Nucl. Instrum. Meth. **A506** (2003) 250.
- [18] M. Clemencic *et al.*, *The LHCb simulation application, Gauss: Design, evolution and experience*, J. Phys. Conf. Ser. **331** (2011) 032023.
- [19] W. D. Hulsbergen, *Decay chain fitting with a Kalman filter*, Nucl. Instrum. Meth. **A552** (2005) 566, [arXiv:physics/0503191](https://arxiv.org/abs/physics/0503191).
- [20] Belle collaboration, K. Abe *et al.*, *Measurement of branching fractions and charge asymmetries for two-body B meson decays with charmonium*, Phys. Rev. **D67** (2003) 032003, [arXiv:hep-ex/0211047](https://arxiv.org/abs/hep-ex/0211047).
- [21] BaBar collaboration, B. Aubert *et al.*, *Measurement of branching fractions and charge asymmetries for exclusive B decays to charmonium*, Phys. Rev. Lett. **94** (2005) 141801, [arXiv:hep-ex/0412062](https://arxiv.org/abs/hep-ex/0412062).
- [22] T. Skwarnicki, *A study of the radiative cascade transitions between the Upsilon-prime and Upsilon resonances*, PhD thesis, Institute of Nuclear Physics, Krakow, 1986, DESY-F31-86-02.
- [23] O. Lupton, L. Anderlini, B. Sciascia, and V. Gligorov, *Calibration samples for particle identification at LHCb in Run 2*, LHCb-PUB-2016-005.
- [24] LHCb collaboration, R. Aaij *et al.*, *Measurement of the track reconstruction efficiency at LHCb*, JINST **10** (2015) P02007, [arXiv:1408.1251](https://arxiv.org/abs/1408.1251).
- [25] LHCb collaboration, R. Aaij *et al.*, *Precision luminosity measurements at LHCb*, JINST **9** (2014) P12005, [arXiv:1410.0149](https://arxiv.org/abs/1410.0149).
- [26] D. Martínez Santos and F. Dupertuis, *Mass distributions marginalized over per-event errors*, Nucl. Instrum. Meth. **A764** (2014) 150, [arXiv:1312.5000](https://arxiv.org/abs/1312.5000).
- [27] M. Cacciari, M. L. Mangano, and P. Nason, *Gluon PDF constraints from the ratio of forward heavy-quark production at the LHC at $\sqrt{s} = 7$ and 13 TeV*, Eur. Phys. J. **C75** (2015) 610, [arXiv:1507.06197](https://arxiv.org/abs/1507.06197).
- [28] P. M. Nadolsky *et al.*, *Implications of CTEQ global analysis for collider observables*, Phys. Rev. **D78** (2008) 013004, [arXiv:0802.0007](https://arxiv.org/abs/0802.0007).

LHCb collaboration

R. Aaij⁴⁰, B. Adeva³⁹, M. Adinolfi⁴⁸, Z. Ajaltouni⁵, S. Akar⁵⁹, J. Albrecht¹⁰, F. Alessio⁴⁰, M. Alexander⁵³, A. Alfonso Albero³⁸, S. Ali⁴³, G. Alkhazov³¹, P. Alvarez Cartelle⁵⁵, A.A. Alves Jr⁵⁹, S. Amato², S. Amerio²³, Y. Amhis⁷, L. An³, L. Anderlini¹⁸, G. Andreassi⁴¹, M. Andreotti^{17,g}, J.E. Andrews⁶⁰, R.B. Appleby⁵⁶, F. Archilli⁴³, P. d'Argent¹², J. Arnau Romeu⁶, A. Artamonov³⁷, M. Artuso⁶¹, E. Aslanides⁶, M. Atzeni⁴², G. Auriemma²⁶, M. Baalouch⁵, I. Babuschkin⁵⁶, S. Bachmann¹², J.J. Back⁵⁰, A. Badalov^{38,m}, C. Baesso⁶², S. Baker⁵⁵, V. Balagura^{7,b}, W. Baldini¹⁷, A. Baranov³⁵, R.J. Barlow⁵⁶, C. Barschel⁴⁰, S. Barsuk⁷, W. Barter⁵⁶, F. Baryshnikov³², V. Batozskaya²⁹, V. Battista⁴¹, A. Bay⁴¹, L. Beauchourt⁴, J. Beddow⁵³, F. Bedeschi²⁴, I. Bediaga¹, A. Beiter⁶¹, L.J. Bel⁴³, N. Beliy⁶³, V. Bellei⁴¹, N. Belloli^{21,i}, K. Belous³⁷, I. Belyaev^{32,40}, E. Ben-Haim⁸, G. Bencivenni¹⁹, S. Benson⁴³, S. Beranek⁹, A. Berezhnoy³³, R. Bernet⁴², D. Berninghoff¹², E. Bertholet⁸, A. Bertolin²³, C. Betancourt⁴², F. Betti¹⁵, M.-O. Bettler⁴⁰, M. van Beuzekom⁴³, Ia. Bezshyiko⁴², S. Bifani⁴⁷, P. Billoir⁸, A. Birnkraut¹⁰, A. Bizzeti^{18,u}, M. Bjørn⁵⁷, T. Blake⁵⁰, F. Blanc⁴¹, S. Blusk⁶¹, V. Bocci²⁶, T. Boettcher⁵⁸, A. Bondar^{36,w}, N. Bondar³¹, I. Bordyuzhin³², S. Borghi⁵⁶, M. Borisjak³⁵, M. Borsato³⁹, F. Bossu⁷, M. Bouabdil⁹, T.J.V. Bowcock⁵⁴, E. Bowen⁴², C. Bozzi^{17,40}, S. Braun¹², T. Britton⁶¹, J. Brodzicka²⁷, D. Brundu¹⁶, E. Buchanan⁴⁸, C. Burr⁵⁶, A. Bursche^{16,f}, J. Buytaert⁴⁰, W. Byczynski⁴⁰, S. Cadeddu¹⁶, H. Cai⁶⁴, R. Calabrese^{17,g}, R. Calladine⁴⁷, M. Calvi^{21,i}, M. Calvo Gomez^{38,m}, A. Camboni^{38,m}, P. Campana¹⁹, D.H. Campora Perez⁴⁰, L. Capriotti⁵⁶, A. Carbone^{15,e}, G. Carboni^{25,j}, R. Cardinale^{20,h}, A. Cardini¹⁶, P. Carniti^{21,i}, L. Carson⁵², K. Carvalho Akiba², G. Casse⁵⁴, L. Cassina²¹, M. Cattaneo⁴⁰, G. Cavallero^{20,40,h}, R. Cenci^{24,t}, D. Chamont⁷, M.G. Chapman⁴⁸, M. Charles⁸, Ph. Charpentier⁴⁰, G. Chatzikonstantinidis⁴⁷, M. Chefdeville⁴, S. Chen¹⁶, S.F. Cheung⁵⁷, S.-G. Chitic⁴⁰, V. Chobanova^{39,40}, M. Chrzaszcz^{42,27}, A. Chubykin³¹, P. Ciambrone¹⁹, X. Cid Vidal³⁹, G. Ciezarek⁴³, P.E.L. Clarke⁵², M. Clemencic⁴⁰, H.V. Cliff⁴⁹, J. Closier⁴⁰, J. Cogan⁶, E. Cogneras⁵, V. Cogoni^{16,f}, L. Cojocariu³⁰, P. Collins⁴⁰, T. Colombo⁴⁰, A. Comerma-Montells¹², A. Contu⁴⁰, A. Cook⁴⁸, G. Coombs⁴⁰, S. Coquereau³⁸, G. Corti⁴⁰, M. Corvo^{17,g}, C.M. Costa Sobral⁵⁰, B. Couturier⁴⁰, G.A. Cowan⁵², D.C. Craik⁵⁸, A. Crocombe⁵⁰, M. Cruz Torres¹, R. Currie⁵², C. D'Ambrosio⁴⁰, F. Da Cunha Marinho², E. Dall'Occo⁴³, J. Dalseno⁴⁸, A. Davis³, O. De Aguiar Francisco⁴⁰, S. De Capua⁵⁶, M. De Cian¹², J.M. De Miranda¹, L. De Paula², M. De Serio^{14,d}, P. De Simone¹⁹, C.T. Dean⁵³, D. Decamp⁴, L. Del Buono⁸, H.-P. Dembinski¹¹, M. Demmer¹⁰, A. Dendek²⁸, D. Derkach³⁵, O. Deschamps⁵, F. Dettori⁵⁴, B. Dey⁶⁵, A. Di Canto⁴⁰, P. Di Nezza¹⁹, H. Dijkstra⁴⁰, F. Dordei⁴⁰, M. Dorigo⁴⁰, A. Dosil Suárez³⁹, L. Douglas⁵³, A. Dovbnya⁴⁵, K. Dreimanis⁵⁴, L. Dufour⁴³, G. Dujany⁸, P. Durante⁴⁰, R. Dzhelyadin³⁷, M. Dziewiecki¹², A. Dziurda⁴⁰, A. Dzyuba³¹, S. Easo⁵¹, M. Ebert⁵², U. Egede⁵⁵, V. Egorychev³², S. Eidelman^{36,w}, S. Eisenhardt⁵², U. Eitschberger¹⁰, R. Ekelhof¹⁰, L. Eklund⁵³, S. Ely⁶¹, S. Esen¹², H.M. Evans⁴⁹, T. Evans⁵⁷, A. Falabella¹⁵, N. Farley⁴⁷, S. Farry⁵⁴, D. Fazzini^{21,i}, L. Federici²⁵, D. Ferguson⁵², G. Fernandez³⁸, P. Fernandez Declara⁴⁰, A. Fernandez Prieto³⁹, F. Ferrari¹⁵, F. Ferreira Rodrigues², M. Ferro-Luzzi⁴⁰, S. Filippov³⁴, R.A. Fini¹⁴, M. Fiorini^{17,g}, M. Firlej²⁸, C. Fitzpatrick⁴¹, T. Fiutowski²⁸, F. Fleuret^{7,b}, K. Fohl⁴⁰, M. Fontana^{16,40}, F. Fontanelli^{20,h}, D.C. Forshaw⁶¹, R. Forty⁴⁰, V. Franco Lima⁵⁴, M. Frank⁴⁰, C. Frei⁴⁰, J. Fu^{22,q}, W. Funk⁴⁰, E. Furfarò^{25,j}, C. Färber⁴⁰, E. Gabriel⁵², A. Gallas Torreira³⁹, D. Galli^{15,e}, S. Gallorini²³, S. Gambetta⁵², M. Gandelman², P. Gandini²², Y. Gao³, L.M. Garcia Martin⁷⁰, J. García Pardiñas³⁹, J. Garra Tico⁴⁹, L. Garrido³⁸, P.J. Garsed⁴⁹, D. Gascon³⁸, C. Gaspar⁴⁰, L. Gavardi¹⁰, G. Gazzoni⁵, D. Gerick¹², E. Gersabeck⁵⁶, M. Gersabeck⁵⁶, T. Gershon⁵⁰, Ph. Ghez⁴, S. Gianì⁴¹, V. Gibson⁴⁹, O.G. Girard⁴¹, L. Giubega³⁰, K. Gizzov⁵², V.V. Gligorov⁸, D. Golubkov³², A. Golutvin⁵⁵, A. Gomes^{1,a}, I.V. Gorelov³³, C. Gotti^{21,i}, E. Govorkova⁴³, J.P. Grabowski¹², R. Graciani Diaz³⁸, L.A. Granado Cardoso⁴⁰, E. Graugés³⁸, E. Graverini⁴²,

G. Graziani¹⁸, A. Grecu³⁰, R. Greim⁹, P. Griffith¹⁶, L. Grillo²¹, L. Gruber⁴⁰,
 B.R. Gruberg Cazon⁵⁷, O. Grünberg⁶⁷, E. Gushchin³⁴, Yu. Guz³⁷, T. Gys⁴⁰, C. Göbel⁶²,
 T. Hadavizadeh⁵⁷, C. Hadjivasilou⁵, G. Haefeli⁴¹, C. Haen⁴⁰, S.C. Haines⁴⁹, B. Hamilton⁶⁰,
 X. Han¹², T.H. Hancock⁵⁷, S. Hansmann-Menzemer¹², N. Harnew⁵⁷, S.T. Harnew⁴⁸, C. Hasse⁴⁰,
 M. Hatch⁴⁰, J. He⁶³, M. Hecker⁵⁵, K. Heinicke¹⁰, A. Heister⁹, K. Hennessy⁵⁴, P. Henrard⁵,
 L. Henry⁷⁰, E. van Herwijnen⁴⁰, M. Heß⁶⁷, A. Hicheur², D. Hill⁵⁷, C. Hombach⁵⁶,
 P.H. Hopchev⁴¹, W. Hu⁶⁵, Z.C. Huard⁵⁹, W. Hulsbergen⁴³, T. Humair⁵⁵, M. Hushchyn³⁵,
 D. Hutchcroft⁵⁴, P. Ibis¹⁰, M. Idzik²⁸, P. Ilten⁵⁸, R. Jacobsson⁴⁰, J. Jalocha⁵⁷, E. Jans⁴³,
 A. Jawahery⁶⁰, F. Jiang³, M. John⁵⁷, D. Johnson⁴⁰, C.R. Jones⁴⁹, C. Joram⁴⁰, B. Jost⁴⁰,
 N. Jurik⁵⁷, S. Kandybei⁴⁵, M. Karacson⁴⁰, J.M. Kariuki⁴⁸, S. Karodia⁵³, N. Kazeev³⁵,
 M. Kecke¹², F. Keizer⁴⁹, M. Kelsey⁶¹, M. Kenzie⁴⁹, T. Ketel⁴⁴, E. Khairullin³⁵, B. Khanji¹²,
 C. Khurewathanakul⁴¹, T. Kirn⁹, S. Klaver⁵⁶, K. Klimaszewski²⁹, T. Klimkovich¹¹, S. Koliiev⁴⁶,
 M. Kolpin¹², R. Kopecna¹², P. Koppenburg⁴³, A. Kosmyntseva³², S. Kotriakhova³¹,
 M. Kozeiha⁵, L. Kravchuk³⁴, M. Kreps⁵⁰, F. Kress⁵⁵, P. Krokovny^{36,w}, F. Kruse¹⁰,
 W. Krzemien²⁹, W. Kucewicz^{27,l}, M. Kucharczyk²⁷, V. Kudryavtsev^{36,w}, A.K. Kuonen⁴¹,
 T. Kvaratskheliya^{32,40}, D. Lacarrere⁴⁰, G. Lafferty⁵⁶, A. Lai¹⁶, G. Lanfranchi¹⁹,
 C. Langenbruch⁹, T. Latham⁵⁰, C. Lazzeroni⁴⁷, R. Le Gac⁶, A. Leflat^{33,40}, J. Lefrançois⁷,
 R. Lefèvre⁵, F. Lemaitre⁴⁰, E. Lemos Cid³⁹, O. Leroy⁶, T. Lesiak²⁷, B. Leverington¹², P.-R. Li⁶³,
 T. Li³, Y. Li⁷, Z. Li⁶¹, T. Likhomanenko⁶⁸, R. Lindner⁴⁰, F. Lionetto⁴², V. Lisovskyi⁷, X. Liu³,
 D. Loh⁵⁰, A. Loi¹⁶, I. Longstaff⁵³, J.H. Lopes², D. Lucchesi^{23,o}, M. Lucio Martinez³⁹, H. Luo⁵²,
 A. Lupato²³, E. Luppi^{17,g}, O. Lupton⁴⁰, A. Lusiani²⁴, X. Lyu⁶³, F. Machefert⁷, F. Maciuc³⁰,
 V. Macko⁴¹, P. Mackowiak¹⁰, S. Maddrell-Mander⁴⁸, O. Maev^{31,40}, K. Maguire⁵⁶,
 D. Maisuzenko³¹, M.W. Majewski²⁸, S. Malde⁵⁷, B. Malecki²⁷, A. Malinin⁶⁸, T. Maltsev^{36,w},
 G. Manca^{16,f}, G. Mancinelli⁶, D. Marangotto^{22,q}, J. Maratas^{5,v}, J.F. Marchand⁴, U. Marconi¹⁵,
 C. Marin Benito³⁸, M. Marinangeli⁴¹, P. Marino⁴¹, J. Marks¹², G. Martellotti²⁶, M. Martin⁶,
 M. Martinelli⁴¹, D. Martinez Santos³⁹, F. Martinez Vidal⁷⁰, L.M. Massacrier⁷, A. Massafferri¹,
 R. Matev⁴⁰, A. Mathad⁵⁰, Z. Mathe⁴⁰, C. Matteuzzi²¹, A. Mauri⁴², E. Maurice^{7,b}, B. Maurin⁴¹,
 A. Mazurov⁴⁷, M. McCann^{55,40}, A. McNab⁵⁶, R. McNulty¹³, J.V. Mead⁵⁴, B. Meadows⁵⁹,
 C. Meaux⁶, F. Meier¹⁰, N. Meinert⁶⁷, D. Melnychuk²⁹, M. Merk⁴³, A. Merli^{22,40,q},
 E. Michielin²³, D.A. Milanes⁶⁶, E. Millard⁵⁰, M.-N. Minard⁴, L. Minzoni¹⁷, D.S. Mitzel¹²,
 A. Mogini⁸, J. Molina Rodriguez¹, T. Mombächer¹⁰, I.A. Monroy⁶⁶, S. Monteil⁵,
 M. Morandin²³, M.J. Morello^{24,t}, O. Morgunova⁶⁸, J. Moron²⁸, A.B. Morris⁵², R. Mountain⁶¹,
 F. Muheim⁵², M. Mulder⁴³, D. Müller⁵⁶, J. Müller¹⁰, K. Müller⁴², V. Müller¹⁰, P. Naik⁴⁸,
 T. Nakada⁴¹, R. Nandakumar⁵¹, A. Nandi⁵⁷, I. Nasteva², M. Needham⁵², N. Neri^{22,40},
 S. Neubert¹², N. Neufeld⁴⁰, M. Neuner¹², T.D. Nguyen⁴¹, C. Nguyen-Mau^{41,n}, S. Nieswand⁹,
 R. Niet¹⁰, N. Nikitin³³, T. Nikodem¹², A. Nogay⁶⁸, D.P. O'Hanlon⁵⁰, A. Oblakowska-Mucha²⁸,
 V. Obraztsov³⁷, S. Ogilvy¹⁹, R. Oldeman^{16,f}, C.J.G. Onderwater⁷¹, A. Ossowska²⁷,
 J.M. Otalora Goicochea², P. Owen⁴², A. Oyanguren⁷⁰, P.R. Pais⁴¹, A. Palano¹⁴,
 M. Palutan^{19,40}, A. Papanestis⁵¹, M. Pappagallo^{14,d}, L.L. Pappalardo^{17,g}, W. Parker⁶⁰,
 C. Parkes⁵⁶, G. Passaleva^{18,40}, A. Pastore^{14,d}, M. Patel⁵⁵, C. Patrignani^{15,e}, A. Pearce⁴⁰,
 A. Pellegrino⁴³, G. Penso²⁶, M. Pepe Altarelli⁴⁰, S. Perazzini⁴⁰, P. Perret⁵, L. Pescatore⁴¹,
 K. Petridis⁴⁸, A. Petrolini^{20,h}, A. Petrov⁶⁸, M. Petruzzo^{22,q}, E. Picatoste Olloqui³⁸,
 B. Pietrzyk⁴, M. Pikies²⁷, D. Pinci²⁶, F. Pisani⁴⁰, A. Pistone^{20,h}, A. Piucci¹², V. Placinta³⁰,
 S. Playfer⁵², M. Plo Casasus³⁹, F. Polci⁸, M. Poli Lener¹⁹, A. Poluektov⁵⁰, I. Polyakov⁶¹,
 E. Polycarpo², G.J. Pomery⁴⁸, S. Ponce⁴⁰, A. Popov³⁷, D. Popov^{11,40}, S. Poslavskii³⁷,
 C. Potterat², E. Price⁴⁸, J. Prisciandaro³⁹, C. Prouve⁴⁸, V. Pugatch⁴⁶, A. Puig Navarro⁴²,
 H. Pullen⁵⁷, G. Punzi^{24,p}, W. Qian⁵⁰, R. Quagliani^{7,48}, B. Quintana⁵, B. Rachwal²⁸,
 J.H. Rademacker⁴⁸, M. Rama²⁴, M. Ramos Pernas³⁹, M.S. Rangel², I. Raniuk^{45,†},
 F. Ratnikov³⁵, G. Raven⁴⁴, M. Ravonel Salzgeber⁴⁰, M. Reboud⁴, F. Redi⁵⁵, S. Reichert¹⁰,
 A.C. dos Reis¹, C. Remon Alepuz⁷⁰, V. Renaudin⁷, S. Ricciardi⁵¹, S. Richards⁴⁸, M. Rihl⁴⁰,

K. Rinnert⁵⁴, V. Rives Molina³⁸, P. Robbe⁷, A. Robert⁸, A.B. Rodrigues¹, E. Rodrigues⁵⁹,
 J.A. Rodriguez Lopez⁶⁶, A. Rogozhnikov³⁵, S. Roiser⁴⁰, A. Rollings⁵⁷, V. Romanovskiy³⁷,
 A. Romero Vidal³⁹, J.W. Ronayne¹³, M. Rotondo¹⁹, M.S. Rudolph⁶¹, T. Ruf⁴⁰, P. Ruiz Valls⁷⁰,
 J. Ruiz Vidal⁷⁰, J.J. Saborido Silva³⁹, E. Sadykhov³², N. Sagidova³¹, B. Saitta^{16,f},
 V. Salustino Guimaraes⁶², C. Sanchez Mayordomo⁷⁰, B. Sanmartin Sedes³⁹, R. Santacesaria²⁶,
 C. Santamarina Rios³⁹, M. Santimaria¹⁹, E. Santovetti^{25,j}, G. Sarpis⁵⁶, A. Sarti^{19,k},
 C. Satriano^{26,s}, A. Satta²⁵, D.M. Saunders⁴⁸, D. Savrina^{32,33}, S. Schael⁹, M. Schellenberg¹⁰,
 M. Schiller⁵³, H. Schindler⁴⁰, M. Schmelling¹¹, T. Schmelzer¹⁰, B. Schmidt⁴⁰, O. Schneider⁴¹,
 A. Schopper⁴⁰, H.F. Schreiner⁵⁹, M. Schubiger⁴¹, M.-H. Schune⁷, R. Schwemmer⁴⁰,
 B. Sciascia¹⁹, A. Sciubba^{26,k}, A. Semennikov³², E.S. Sepulveda⁸, A. Sergi⁴⁷, N. Serra⁴²,
 J. Serrano⁶, L. Sestini²³, P. Seyfert⁴⁰, M. Shapkin³⁷, I. Shapoval⁴⁵, Y. Shcheglov³¹, T. Shears⁵⁴,
 L. Shekhtman^{36,w}, V. Shevchenko⁶⁸, B.G. Siddi¹⁷, R. Silva Coutinho⁴², L. Silva de Oliveira²,
 G. Simi^{23,o}, S. Simone^{14,d}, M. Sirendi⁴⁹, N. Skidmore⁴⁸, T. Skwarnicki⁶¹, E. Smith⁵⁵,
 I.T. Smith⁵², J. Smith⁴⁹, M. Smith⁵⁵, I. Soares Lavra¹, M.D. Sokoloff⁵⁹, F.J.P. Soler⁵³,
 B. Souza De Paula², B. Spaan¹⁰, P. Spradlin⁵³, S. Sridharan⁴⁰, F. Stagni⁴⁰, M. Stahl¹²,
 S. Stahl⁴⁰, P. Steffko⁴¹, S. Stefkova⁵⁵, O. Steinkamp⁴², S. Stemmle¹², O. Stenyakin³⁷,
 M. Stepanova³¹, H. Stevens¹⁰, S. Stone⁶¹, B. Storaci⁴², S. Stracka^{24,p}, M.E. Stramaglia⁴¹,
 M. Straticiuc³⁰, U. Straumann⁴², J. Sun³, L. Sun⁶⁴, W. Sutcliffe⁵⁵, K. Swientek²⁸,
 V. Syropoulos⁴⁴, T. Szumlak²⁸, M. Szymanski⁶³, S. T'Jampens⁴, A. Tayduganov⁶,
 T. Tekampe¹⁰, G. Tellarini^{17,g}, F. Teubert⁴⁰, E. Thomas⁴⁰, J. van Tilburg⁴³, M.J. Tilley⁵⁵,
 V. Tisserand⁴, M. Tobin⁴¹, S. Tolk⁴⁹, L. Tomassetti^{17,g}, D. Tonelli²⁴, F. Toriello⁶¹,
 R. Tourinho Jadallah Aoude¹, E. Tournefier⁴, M. Traili⁵³, M.T. Tran⁴¹, M. Tresch⁴²,
 A. Trisovic⁴⁰, A. Tsaregorodtsev⁶, P. Tsopelas⁴³, A. Tully⁴⁹, N. Tuning^{43,40}, A. Ukleja²⁹,
 A. Usachov⁷, A. Ustyuzhanin³⁵, U. Uwer¹², C. Vacca^{16,f}, A. Vagner⁶⁹, V. Vagnoni^{15,40},
 A. Valassi⁴⁰, S. Valat⁴⁰, G. Valenti¹⁵, R. Vazquez Gomez⁴⁰, P. Vazquez Regueiro³⁹, S. Vecchi¹⁷,
 M. van Veghel⁴³, J.J. Velthuis⁴⁸, M. Veltri^{18,r}, G. Veneziano⁵⁷, A. Venkateswaran⁶¹,
 T.A. Verlage⁹, M. Vernet⁵, M. Vesterinen⁵⁷, J.V. Viana Barbosa⁴⁰, B. Viaud⁷, D. Vieira⁶³,
 M. Vieites Diaz³⁹, H. Viemann⁶⁷, X. Vilasis-Cardona^{38,m}, M. Vitti⁴⁹, V. Volkov³³,
 A. Vollhardt⁴², B. Voneki⁴⁰, A. Vorobyev³¹, V. Vorobyev^{36,w}, C. Voß⁹, J.A. de Vries⁴³,
 C. Vázquez Sierra³⁹, R. Waldi⁶⁷, C. Wallace⁵⁰, R. Wallace¹³, J. Walsh²⁴, J. Wang⁶¹,
 D.R. Ward⁴⁹, H.M. Wark⁵⁴, N.K. Watson⁴⁷, D. Websdale⁵⁵, A. Weiden⁴², C. Weisser⁵⁸,
 M. Whitehead⁴⁰, J. Wicht⁵⁰, G. Wilkinson⁵⁷, M. Wilkinson⁶¹, M. Williams⁵⁶, M.P. Williams⁴⁷,
 M. Williams⁵⁸, T. Williams⁴⁷, F.F. Wilson^{51,40}, J. Wimberley⁶⁰, M. Winn⁷, J. Wishahi¹⁰,
 W. Wislicki²⁹, M. Witek²⁷, G. Wormser⁷, S.A. Wotton⁴⁹, K. Wraight⁵³, K. Wyllie⁴⁰, Y. Xie⁶⁵,
 M. Xu⁶⁵, Z. Xu⁴, Z. Yang³, Z. Yang⁶⁰, Y. Yao⁶¹, H. Yin⁶⁵, J. Yu⁶⁵, X. Yuan⁶¹,
 O. Yushchenko³⁷, K.A. Zarebski⁴⁷, M. Zavertyaev^{11,c}, L. Zhang³, Y. Zhang⁷, A. Zhelezov¹²,
 Y. Zheng⁶³, X. Zhu³, V. Zhukov³³, J.B. Zonneveld⁵², S. Zucchelli¹⁵.

¹Centro Brasileiro de Pesquisas Físicas (CBPF), Rio de Janeiro, Brazil

²Universidade Federal do Rio de Janeiro (UFRJ), Rio de Janeiro, Brazil

³Center for High Energy Physics, Tsinghua University, Beijing, China

⁴LAPP, Université Savoie Mont-Blanc, CNRS/IN2P3, Annecy-Le-Vieux, France

⁵Clermont Université, Université Blaise Pascal, CNRS/IN2P3, LPC, Clermont-Ferrand, France

⁶Aix Marseille Univ, CNRS/IN2P3, CPPM, Marseille, France

⁷LAL, Université Paris-Sud, CNRS/IN2P3, Orsay, France

⁸LPNHE, Université Pierre et Marie Curie, Université Paris Diderot, CNRS/IN2P3, Paris, France

⁹I. Physikalisches Institut, RWTH Aachen University, Aachen, Germany

¹⁰Fakultät Physik, Technische Universität Dortmund, Dortmund, Germany

¹¹Max-Planck-Institut für Kernphysik (MPIK), Heidelberg, Germany

¹²Physikalisches Institut, Ruprecht-Karls-Universität Heidelberg, Heidelberg, Germany

¹³School of Physics, University College Dublin, Dublin, Ireland

¹⁴Sezione INFN di Bari, Bari, Italy

- ¹⁵Sezione INFN di Bologna, Bologna, Italy
¹⁶Sezione INFN di Cagliari, Cagliari, Italy
¹⁷Università e INFN, Ferrara, Ferrara, Italy
¹⁸Sezione INFN di Firenze, Firenze, Italy
¹⁹Laboratori Nazionali dell'INFN di Frascati, Frascati, Italy
²⁰Sezione INFN di Genova, Genova, Italy
²¹Università & INFN, Milano-Bicocca, Milano, Italy
²²Sezione di Milano, Milano, Italy
²³Sezione INFN di Padova, Padova, Italy
²⁴Sezione INFN di Pisa, Pisa, Italy
²⁵Sezione INFN di Roma Tor Vergata, Roma, Italy
²⁶Sezione INFN di Roma La Sapienza, Roma, Italy
²⁷Henryk Niewodniczanski Institute of Nuclear Physics Polish Academy of Sciences, Kraków, Poland
²⁸AGH - University of Science and Technology, Faculty of Physics and Applied Computer Science, Kraków, Poland
²⁹National Center for Nuclear Research (NCBJ), Warsaw, Poland
³⁰Horia Hulubei National Institute of Physics and Nuclear Engineering, Bucharest-Magurele, Romania
³¹Petersburg Nuclear Physics Institute (PNPI), Gatchina, Russia
³²Institute of Theoretical and Experimental Physics (ITEP), Moscow, Russia
³³Institute of Nuclear Physics, Moscow State University (SINP MSU), Moscow, Russia
³⁴Institute for Nuclear Research of the Russian Academy of Sciences (INR RAN), Moscow, Russia
³⁵Yandex School of Data Analysis, Moscow, Russia
³⁶Budker Institute of Nuclear Physics (SB RAS), Novosibirsk, Russia
³⁷Institute for High Energy Physics (IHEP), Protvino, Russia
³⁸ICCUB, Universitat de Barcelona, Barcelona, Spain
³⁹Universidad de Santiago de Compostela, Santiago de Compostela, Spain
⁴⁰European Organization for Nuclear Research (CERN), Geneva, Switzerland
⁴¹Institute of Physics, Ecole Polytechnique Fédérale de Lausanne (EPFL), Lausanne, Switzerland
⁴²Physik-Institut, Universität Zürich, Zürich, Switzerland
⁴³Nikhef National Institute for Subatomic Physics, Amsterdam, The Netherlands
⁴⁴Nikhef National Institute for Subatomic Physics and VU University Amsterdam, Amsterdam, The Netherlands
⁴⁵NSC Kharkiv Institute of Physics and Technology (NSC KIPT), Kharkiv, Ukraine
⁴⁶Institute for Nuclear Research of the National Academy of Sciences (KINR), Kyiv, Ukraine
⁴⁷University of Birmingham, Birmingham, United Kingdom
⁴⁸H.H. Wills Physics Laboratory, University of Bristol, Bristol, United Kingdom
⁴⁹Cavendish Laboratory, University of Cambridge, Cambridge, United Kingdom
⁵⁰Department of Physics, University of Warwick, Coventry, United Kingdom
⁵¹STFC Rutherford Appleton Laboratory, Didcot, United Kingdom
⁵²School of Physics and Astronomy, University of Edinburgh, Edinburgh, United Kingdom
⁵³School of Physics and Astronomy, University of Glasgow, Glasgow, United Kingdom
⁵⁴Oliver Lodge Laboratory, University of Liverpool, Liverpool, United Kingdom
⁵⁵Imperial College London, London, United Kingdom
⁵⁶School of Physics and Astronomy, University of Manchester, Manchester, United Kingdom
⁵⁷Department of Physics, University of Oxford, Oxford, United Kingdom
⁵⁸Massachusetts Institute of Technology, Cambridge, MA, United States
⁵⁹University of Cincinnati, Cincinnati, OH, United States
⁶⁰University of Maryland, College Park, MD, United States
⁶¹Syracuse University, Syracuse, NY, United States
⁶²Pontifícia Universidade Católica do Rio de Janeiro (PUC-Rio), Rio de Janeiro, Brazil, associated to ²
⁶³University of Chinese Academy of Sciences, Beijing, China, associated to ³
⁶⁴School of Physics and Technology, Wuhan University, Wuhan, China, associated to ³
⁶⁵Institute of Particle Physics, Central China Normal University, Wuhan, Hubei, China, associated to ³
⁶⁶Departamento de Física, Universidad Nacional de Colombia, Bogota, Colombia, associated to ⁸
⁶⁷Institut für Physik, Universität Rostock, Rostock, Germany, associated to ¹²
⁶⁸National Research Centre Kurchatov Institute, Moscow, Russia, associated to ³²

⁶⁹*National Research Tomsk Polytechnic University, Tomsk, Russia, associated to* ³²

⁷⁰*Instituto de Fisica Corpuscular, Centro Mixto Universidad de Valencia - CSIC, Valencia, Spain, associated to* ³⁸

⁷¹*Van Swinderen Institute, University of Groningen, Groningen, The Netherlands, associated to* ⁴³

^a*Universidade Federal do Triângulo Mineiro (UFTM), Uberaba-MG, Brazil*

^b*Laboratoire Leprince-Ringuet, Palaiseau, France*

^c*P.N. Lebedev Physical Institute, Russian Academy of Science (LPI RAS), Moscow, Russia*

^d*Università di Bari, Bari, Italy*

^e*Università di Bologna, Bologna, Italy*

^f*Università di Cagliari, Cagliari, Italy*

^g*Università di Ferrara, Ferrara, Italy*

^h*Università di Genova, Genova, Italy*

ⁱ*Università di Milano Bicocca, Milano, Italy*

^j*Università di Roma Tor Vergata, Roma, Italy*

^k*Università di Roma La Sapienza, Roma, Italy*

^l*AGH - University of Science and Technology, Faculty of Computer Science, Electronics and Telecommunications, Kraków, Poland*

^m*LIFAELS, La Salle, Universitat Ramon Llull, Barcelona, Spain*

ⁿ*Hanoi University of Science, Hanoi, Viet Nam*

^o*Università di Padova, Padova, Italy*

^p*Università di Pisa, Pisa, Italy*

^q*Università degli Studi di Milano, Milano, Italy*

^r*Università di Urbino, Urbino, Italy*

^s*Università della Basilicata, Potenza, Italy*

^t*Scuola Normale Superiore, Pisa, Italy*

^u*Università di Modena e Reggio Emilia, Modena, Italy*

^v*Iligan Institute of Technology (IIT), Iligan, Philippines*

^w*Novosibirsk State University, Novosibirsk, Russia*

[†]*Deceased*